fractal and fractional

MDPI

Article

Event-Triggered Sampled-Data Iterative Learning Control for Fractional-Order Cyber-Physical Systems

Jiajun Sun [1], Siyuan Wang [1], Xingyu Zhou [1,*], Xinsong Zhang [1] and Chenghong Gu [2,*]

[1] School of Electrical Engineering and Automation, Nantong University, Nantong 226019, China
[2] Department of Electrical and Electronic Engineering, University of Bath, Bath BA2 7AY, UK
* Correspondence: staryuz@ntu.edu.cn (X.Z.); c.gu@bath.ac.uk (C.G.)

Abstract

This paper investigates the output synchronization of fractional-order cyber-physical systems (FOCPSs) under communication constraints. To address limited bandwidth and high transmission costs, an event-triggered encoding-decoding sampled-data iterative learning control (ET-EDSDILC) protocol is proposed. The control law integrates a quantized sampling framework with an encoding–decoding mechanism to reconstruct control signals and address communication constraints. Furthermore, an event-triggered mechanism based on error energy attenuation (EEA) is developed to adjust communication frequency by monitoring error trends, thereby reducing unnecessary data transmissions. By applying fractional-order calculus and the contraction mapping principle, sufficient conditions for output synchronization are derived. Numerical simulations show that the proposed ET-EDSDILC framework reduces communication overhead and data redundancy while maintaining tracking performance, offering a solution for FOCPSs under communication constraints.

Keywords: fractional-order cyber-physical systems; event-triggered mechanism; encoding-decoding mechanism; iterative learning control; output synchronization; sampled-data control

1. Introduction

In recent decades, the collective behaviors and coordinated control of cyber-physical systems (CPSs) have emerged as a focal point of multidisciplinary research, owing to their extensive deployment in smart grids [1], autonomous vehicle platoons [2], and wireless sensor networks [3,4]. A fundamental objective within these networked architectures is consensus synchronization, where interconnected nodes aim to achieve state consistency through localized information exchange. In practical engineering environments, many physical processes exhibit intrinsic memory and hereditary properties that are not fully captured by classical integer-order models. Fractional calculus accurately captures complex dynamics due to its inherent non-locality and memory effects [5–7]. This framework offers an extra degree of freedom through its non-integer differentiation order, allowing for more precise characterization of the "history-dependent" nature of complex systems. This mathematical flexibility is particularly crucial for modeling phenomena where historical states continuously shape future dynamics, such as the viscoelasticity in robotic joints, the electrochemical reactions in smart grid storage [8], and the long-range dependence in transportation networks [9]. Consequently, investigating the output synchronization issues

Check for updates

Academic Editor: Haci Mehmet Baskonus

Received: 3 May 2026
Revised: 12 June 2026
Accepted: 16 June 2026
Published: 18 June 2026

Copyright: © 2026 by the authors. Licensee MDPI, Basel, Switzerland. This article is an open access article distributed under the terms and conditions of the Creative Commons Attribution (CC BY) license.

of fractional-order cyber-physical systems (FOCPSs) is of significant theoretical value and practical importance.

Iterative learning control (ILC) has proven to be an effective paradigm for networked systems required to execute output synchronization tasks repetitively over a finite time interval. Reference [10] investigated the ILC design for systems lacking a priori knowledge of the control direction. Reference [11] focused on the development of monotonically convergent ILC for linear discrete-time systems, while Reference [12] explored the convergence properties of ILC in SISO nonrepetitive systems affected by iteration-dependent uncertainties. To extend this learning framework to non-integer order dynamics, several foundational studies on fractional-order ILC (FOILC) have been established. For instance, the design of FOILC schemes specifically tailored for fractional-order linear architectures was pioneered in [13], which provided the theoretical basis for non-integer order learning laws. Furthermore, considering the complex characteristics in practical systems, the Reference [14] addressed the tracking control problem for fractional-order linear systems with time delay by virtue of a rigorous frequency analysis approach. Specifically, the inherent repetitive nature of operation cycles in CPS is exploited by ILC algorithms, through which tracking errors and periodic disturbances are progressively attenuated over successive iterations to ensure superior execution precision [15,16]. By incorporating tracking information from previous executions to refine current control signals, ILC facilitates high-precision performance for systems operating in a repetitive manner. However, the practical implementation of ILC in modern networked environments often faces significant challenges related to communication efficiency [17,18]. The continuous exchange of high-resolution information across the network can place an excessive burden on limited communication bandwidth and computational resources. Mitigating this communication pressure while maintaining convergence performance is critical for the efficient deployment of large-scale FOCPSs.

To address these bandwidth constraints, sampled-data control and event-triggered mechanisms have been widely considered as viable strategies [19–21]. Furthermore, in digital communication channels, signal quantization—where continuous signals are mapped to discrete levels—is often a practical necessity [18,22]. To further enhance data security and transmission reliability, the integration of encoding and decoding mechanisms has gained attention, as they can effectively reconstruct control information and mitigate the impact of communication uncertainties [23,24]. While fixed-period sampling provides a basic digital framework, it may still involve redundant data transmissions. Non-periodic event-triggered control offers a more flexible approach. Specifically, the error energy attenuation (EEA)-based event-triggered mechanism provides a sophisticated alternative by regulating control updates based on the dissipation rate of output synchronization error energy, thereby offering a more nuanced way to manage communication overhead [25].

Motivated by these considerations, this study investigates the output synchronization problem of FOCPSs under an event-triggered encoding-decoding sampled-data iterative learning control (ET-EDSDILC) protocol. This work explores the integration of an EEA-based triggering mechanism and an encoding–decoding framework into the iterative learning process of fractional-order systems subject to communication constraints. Specifically, an ILC law incorporating quantized sampling and encoding–decoding stages is synthesized, where control trajectories are updated solely based on processed discrete error fragments. The communication frequency is dynamically regulated by the orchestrated EEA-based mechanism, pruning redundant iterations while striving to maintain the strict output synchronization of the system states.

The primary contributions of this work are summarized as follows

(i) In contrast to the general integer-order frameworks widely investigated in recent literature, the specific mathematical complexities and hereditary characteristics introduced

by fractional calculus are accommodated within the designed control framework. A sampled-data-based iterative learning control protocol is extended and applied to FOCPSs.

(ii) An event-triggered mechanism and an encoding–decoding mechanism are integrated into the control protocol. The incorporation of these mechanisms is intended to alleviate the network communication burden and mitigate quantization errors, respectively.

(iii) By utilizing the properties of the Mittag–Leffler function and the contraction mapping principle, sufficient criteria for the consensus synchronization of FOCPSs are analytically established. Consequently, the theoretical feasibility and convergence of the proposed control protocol are mathematically verified.

The remainder of this paper is organized as follows. Section 2 introduces mathematical preliminaries. Section 3 describes the FOCPS model and control objectives. Section 4 details the design of the ET-EDSDILC protocol and the EEA-based event-triggered mechanism. Output synchronization analysis is presented in Section 5. Numerical simulations and conclusions are provided in Section 6 and Section 7, respectively.

Notations: $\mathbb{R}^n$ stands for n-dimensional Euclidean space. The transpose of matrix Q is expressed by Q^T. $\otimes$ is the Kronecker product. The symbol I_q denotes the identity matrix with $q \times q$ dimension. For a matrix $Q \in \mathbb{R}^q$, its matrix norm can be defined by $\|Q\| = \sqrt{\lambda_{\max}(Q^{\mathrm{T}}Q)}$, where $\lambda_{\max}(\cdot)$ is the maximum eigenvalue of Q. If $f(t) : [0, T] \to \mathbb{R}^n$ is a vector function, the λ-norm of $f(t)$ is defined as $\|f\|_\lambda = \sup_{t\in[0,T]} \{e^{-\lambda t}\|f(t)\|\}$. Define the ∞-norm as $\|f\|_\infty = \max_{t\in[0,T]} \{\|f(t)\|\}$. $\lfloor\cdot\rfloor$ represent the floor function. 1_N denotes an $N \times 1$ vector of ones.

2. Preliminaries

2.1. Graph Theory

The communication topology among agents in FOCPSs is modeled by a directed graph $\mathcal{G} = (\Lambda, \mathcal{E}, \Theta)$. Here, $\Lambda = \{1, 2, \ldots, N\}$ denotes the node set, and $\mathcal{E} \subseteq \Lambda \times \Lambda$ represents the edge set, where a directed link $(i, j) \in \mathcal{E}$ indicates that information flows from node i to node j. The associated adjacency matrix $\Theta = [a_{ij}]_{N\times N}$ is defined with elements $a_{ij} = 1$ if $(j, i) \in \mathcal{E}$ and $a_{ij} = 0$ otherwise, with $a_{ii} = 0$ for all $i \in \Lambda$.

The Laplacian matrix $\mathcal{L} = [l_{ij}]_{N\times N}$ of digraph is given as follows

$$l_{ij} = \begin{cases} -a_{ij}, & i \neq j, \\ \sum_{k=1,k\neq i}^{N} a_{ik} = \Omega_i, & i = j. \end{cases}$$

The in-degree associated with the i-th node is denoted by Ω_i. Accordingly, a diagonal configuration is employed to define the degree matrix $\Omega = \mathrm{diag}\{\Omega_1, \ldots, \Omega_N\}$, from which the relation $\mathcal{L} = \Omega - \Theta$ is derived. Furthermore, the existence of a spanning tree within a directed graph is established if a root node is identified such that a directed path can be utilized to reach every remaining node from this origin.

2.2. Fractional-Order Calculus

The scope of classical calculus is expanded by fractional-order calculus, through which the fundamental operations of integration and differentiation are generalized to encompass non-integer orders.

Definition 1 ([26]). *Given a function $g(t) : \mathbb{R}^+ \mapsto \mathbb{R}$, the Riemann-Liouville fractional-order integral of order $\alpha > 0$ is formulated as follows*

$$ {}_{t_0}\mathscr{D}_t^{-\alpha} g(t) \triangleq \frac{1}{\Xi(\alpha)} \int_{t_0}^{t} (t-s)^{\alpha-1} g(s) ds, $$

wherein the Gamma function is denoted by the symbol $\Xi(\cdot)$.

Definition 2 ([27]). *For* $\alpha > 0$*, the Caputo fractional derivative is defined by*

$$ {}_{t_0}^{C}\mathscr{D}_t^{\alpha} g(t) \triangleq {}_{t_0}\mathscr{D}_t^{\alpha-\varsigma} g(t) \mathscr{D}^{\varsigma} g(t), \quad \varsigma - 1 \leq \alpha < \varsigma, \varsigma \in \mathbb{N}. $$

For simplicity, $\mathscr{D}_t^{\alpha}$ *denotes the Caputo derivative* ${}_{t_0}^{C}\mathscr{D}_t^{\alpha}$ *hereafter.*

Definition 3 ([28]). *The two-parameter Mittag-Leffler function is defined as follows*

$$ E_{\alpha,\beta}(z) = \sum_{k=0}^{\infty} \frac{z^k}{\Xi(\alpha k + \beta)}, \quad \alpha > 0, \beta > 0, z \in \mathbb{C}. $$

Several fundamental lemmas are recalled for the subsequent stability and synchronization analysis.

Lemma 1 ([28]). *For the Mittag–Leffler function, fractional integration or differentiation satisfies the following identity*

$$ {}_{t_0}\mathscr{D}_t^{\vartheta} \left[t^{\beta-1} E_{\alpha,\beta}(\lambda t^{\alpha}) \right] = t^{\beta-\vartheta-1} E_{\alpha,\beta-\vartheta}(\lambda t^{\alpha}), \quad \vartheta < \beta. $$

Lemma 2 ([29]). *Suppose that continuity is assumed for a function* $u(t)$ *defined on* $t \in [t_0, T]$*, and let* $v(t-\tau)$ *be a continuous, non-negative mapping on the domain* $t_0 \leq \tau \leq T$*. Furthermore, a positive, continuous, and non-declining function is denoted by* $w(t)$ *for* $t \in [t_0, T]$*.*

If

$$ u(t) \leq w(t) + \int_{t_0}^{t} v(t-\tau) u(\tau) d\tau, \quad t \in [t_0, T], $$

then

$$ u(t) \leq w(t) e^{\int_{t_0}^{t} v(t-\tau) d\tau}, \quad t \in [t_0, T]. $$

Lemma 3 ([27]). *Under the assumption that continuity is maintained for the function* $f(t, x(t))$*, an equivalence is established between the following initial value problem*

$$ \begin{cases} {}_{t}^{C}\mathscr{D}_t^{\alpha} x(t) = f(t, x(t)), & 0 < \alpha < 1 \\ x(t_0) = x(0), \end{cases} $$

and the nonlinear Volterra integral equation formulated as

$$ x(t) = x(0) + \frac{1}{\Xi(\alpha)} \int_{t_0}^{t} (t-s)^{\alpha-1} f(s, x(s)) ds, $$

the continuity of the corresponding solutions is guaranteed.

3. System Description and Problem Statement

3.1. The Description of FOCPSs

Consider the following FOCPSs, the i-th ($i \in \Lambda$) agent is described as

$$ \begin{cases} \mathscr{D}_t^{\alpha} x_{i,k}(t) = A x_{i,k}(t) + B u_{i,k}(t), \\ y_{i,k}(t) = C x_{i,k}(t) + D u_{i,k}(t), \end{cases} \tag{1} $$

where $i = 1, 2, \ldots, N$ is the index of nodes. Within this mathematical setup, $\mathcal{D}_t^{\alpha}$ defines the Caputo fractional derivative of order $\alpha \in (0, 1)$. Specifically, the vectors $x_{i,k}(t) \in \mathbb{R}^q$, $u_{i,k}(t) \in \mathbb{R}^m$ and $y_{i,k}(t) \in \mathbb{R}^p$ denote the state, input, and measured output for the i-th agent during the k-th iteration, with system matrices $A \in \mathbb{R}^{q\times q}$, $B \in \mathbb{R}^{q\times m}$, $C \in \mathbb{R}^{p\times q}$ and $D \in \mathbb{R}^{p\times m}$. The ET-EDSDILC investigated in this study—designed for linear FOCPSs—is illustrated in Figure 1.

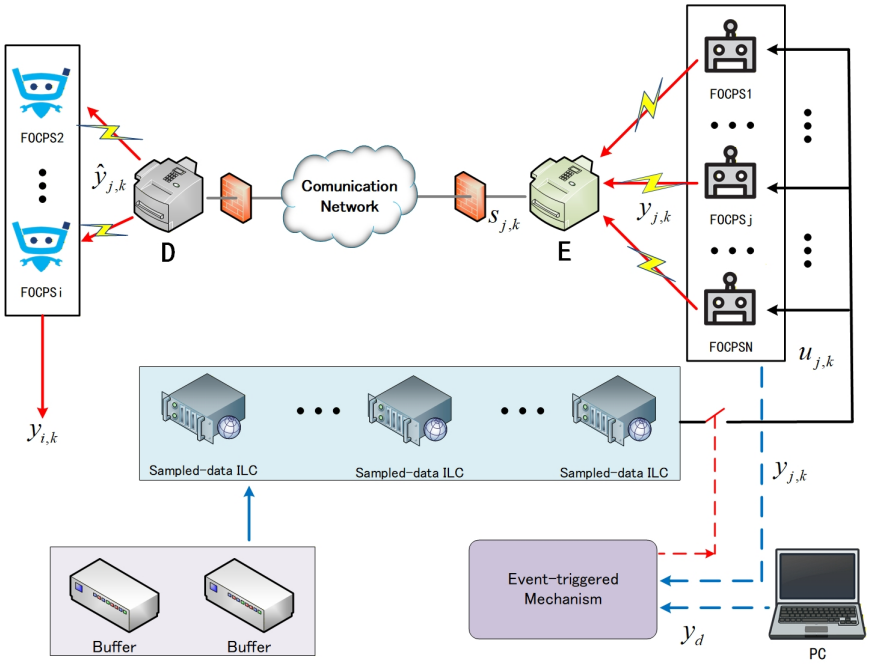


Figure 1. ET-EDSDILC protocol structure for output synchronization of FOCPSs.

To achieve a prescribed output synchronization objective $y_d(t)$ for the FOCPSs over a finite time interval $[0, T]$, the reference manifold is defined as follows

$$\begin{cases} \mathcal{D}_t^{\alpha} x_d(t) = Ax_d(t) + Bu_d(t), \\ y_d(t) = Cx_d(t) + Du_d(t), \end{cases} \tag{2}$$

where $x_d(t)$ represents the desired state. $u_d(t)$ represents the desired control.

This paper aims to synchronize the output trajectories of all FOCPSs with the desired trajectory by designing a distributed protocol that ensures consensus as $k \to \infty$, meaning that

$$\lim_{k\to\infty} \left\| y_{i,k}(t) - y_{j,k}(t) \right\| = 0, \quad \forall t \in [0, T].$$

To facilitate the theoretical analysis, this section presents a fundamental assumption regarding the initial conditions of FOCPSs.

Assumption 1. *The initial conditions of FOCPSs are given by*

$$x_{i,k}(0) = x_d(0), i \in \Lambda.$$

3.2. Quantization and Encoding-Decoding Mechanism of Signals

In the following analysis, we utilize a uniform quantizer defined by

$$\mathcal{Q}(\hbar) = \begin{cases} 0, & \text{if } -\frac{1}{2} < \hbar \leqslant \frac{1}{2}, \\ \omega, & \text{if } \frac{2\omega-1}{2} < \hbar \leqslant \frac{2\omega+1}{2}, \\ -\mathcal{Q}(-\hbar), & \text{if } \hbar \leqslant -\frac{1}{2}, \end{cases} \tag{3}$$

where $\omega = 1, 2, \ldots$ $\mathcal{Q}(\cdot)$ is a map from $\mathbb{R}$ to the set of quantization.

Remark 1. *The uniform quantizer in Equation (3) maps each scalar $\hbar \in \mathbb{R}$ to the quantization level set $\mathbb{Z} = \{0, \pm 1, \pm 2, \ldots\}$, and no overflow occurs since the quantizer is defined over the whole real line. For any $\hbar \in \mathbb{R}$, the quantization error is bounded by $|\hbar - \mathcal{Q}(\hbar)| \leq \frac{1}{2}$. For a vector $\hbar = [\hbar_1, \ldots, \hbar_q]^T$, the quantizer is applied componentwise as $\mathcal{Q}(\hbar) = [\mathcal{Q}(\hbar_1), \ldots, \mathcal{Q}(\hbar_q)]^T$. Hence, $|\hbar_r - \mathcal{Q}(\hbar_r)| \leq \frac{1}{2}$ for $r = 1, 2, \ldots, q$, and the corresponding error vector satisfies $\|\hbar - \mathcal{Q}(\hbar)\| \leq \frac{\sqrt{q}}{2}$.*

The encoding-decoding mechanism (EDM) of signals transmitted between FOCPSs is denoted by $\mathfrak{E}$ and $\mathfrak{D}$. For the j-th ($j \in \Lambda$) agent, the output trajectory $y_{j,k}(t)$ is quantized, transmitted, and subsequently decoded to yield the estimated signal $\hat{y}_{j,k}(t)$. These operations represent the primary mechanism for all inter-agent communication.

The encoder $\mathfrak{E}$ for the j-th FOCPS is formulated as follows

$$\begin{cases} \phi_{j,0}(t) = \mathbf{0}, \\ s_{j,k+1}(t) = \mathcal{Q}\Big(\frac{y_{j,k+1}(t) - \phi_{j,k}(t)}{\beta_k}\Big), \\ \phi_{j,k+1}(t) = \beta_k s_{j,k+1}(t) + \phi_{j,k}(t), \end{cases} \tag{4}$$

where $\mathbf{0}$ denotes the zero vector of appropriate dimensions for $\forall j \in \Lambda, t \in [0, T], k = 0, 1, 2 \ldots$ For encoder $\mathfrak{E}$, $y_{j,k+1}(t)$ and $s_{j,k+1}(t)$ are assigned as the input and output, respectively, while the internal state is represented by $\phi_{j,k+1}(t)$. To augment tracking performance, a scaling sequence $\{\beta_k\}$ is developed. The objective of this design is to modulate the discrepancy between the actual signal and the encoder's internal state. This sequence is governed by $\beta_{k+1} = \mathcal{K}\beta_k$, with $0 < \mathcal{K} < 1$.

Regarding the information transmitted from the j-th agent to the i-th agent, decoder $\mathfrak{D}$ is formulated as follows

$$\begin{cases} \hat{y}_{j,0}(t) = 0, \\ \hat{y}_{j,k+1}(t) = \beta_k s_{j,k+1}(t) + \hat{y}_{j,k}(t), \end{cases} \tag{5}$$

where $\hat{y}_{j,k}(t)$ is the output of decoder $\mathfrak{D}$, which is called the estimated signal, for $\forall j \in \Lambda$, $t \in [0, T], k = 0, 1, 2 \ldots$

Remark 2. *It is assumed that an identical scaling sequence $\{\beta_k\}$ is shared by the EDM of each FOCPS. This uniformity ensures that the same estimated signal is reconstructed from the actual signal following the encoding, transmission, and decoding stages. Consequently, the theoretical framework can be presented in a more concise and unified form.*

From the definitions of decoder and encoder above, the learning control algorithm and the plant dynamics are driven by $\hat{y}_{i,k}(t)$ and $u_{i,k}(t)$. The primary focus of this paper is to investigate the consensus tracking problem for FOCPSs integrated with EDM. Prior to the introduction of the consensus analysis scheme, the relationship between $y_{i,k}(t)$ and $\hat{y}_{i,k}(t)$ is elucidated. By combining Equations (4) and (5), one can get

$$\begin{aligned} \hat{y}_{i,k+1}(t) &= \beta_k s_{i,k+1}(t) + \hat{y}_{i,k}(t) \\ &= y_{i,k+1}(t) - \beta_k \epsilon_{i,k+1}(t) - \phi_{i,k}(t) + \hat{y}_{i,k}(t), \end{aligned} \tag{6}$$

where $\epsilon_{i,k+1}(t) = \Big(\frac{y_{i,k+1}(t) - \phi_{i,k}(t)}{\beta_k}\Big) - \mathcal{Q}\Big(\frac{y_{i,k+1}(t) - \phi_{i,k}(t)}{\beta_k}\Big) \in \mathbb{R}^p$ is the output quantization error. Define $\epsilon_k(t) = [(\epsilon_{1,k}(t))^T, (\epsilon_{2,k}(t))^T, \ldots, (\epsilon_{N,k}(t))^T]^T \in \mathbb{R}^{Np}$. Obviously, there is $\|\epsilon_k\|_\infty \leq \frac{1}{2}\sqrt{Np}$.

The connection between $\hat{y}_{i,k}(t)$ and $\phi_{i,k}(t)$ is established in Equation (6). Based on the formal definition of the EDM, it follows that

$$\begin{aligned}\hat{y}_{i,k+1}(t) - \phi_{i,k+1}(t) &= (\beta_k s_{i,k+1}(t) + \hat{y}_{i,k}(t)) - (\beta_k s_{i,k+1}(t) + \phi_{i,k}(t)) \\ &= \hat{y}_{i,k}(t) - \phi_{i,k}(t).\end{aligned}$$

For the initial iteration, one gets

$$\hat{y}_{i,0}(t) - \phi_{i,0}(t) = 0.$$

By employing the method of mathematical induction, it can be derived that

$$\hat{y}_{i,k}(t) - \phi_{i,k}(t) = 0, \quad \forall k, t \in [0, T]. \tag{7}$$

Combining Equations (6) and (7), one has

$$\begin{cases} \phi_{i,k}(t) = y_{i,k}(t) - \beta_k \epsilon_{i,k}(t), \\ \hat{y}_{i,k}(t) = y_{i,k}(t) - \beta_k \epsilon_{i,k}(t). \end{cases} \tag{8}$$

4. Synchronization Analysis of FOCPSs

4.1. ET-EDSDILC Protocol Design

In the context of continuous-time systems, the duration $[0, T]$ is subdivided by a sampling mechanism into M distinct intervals, each possessing a uniform length h. The collection of sampling indices is represented by the set $n = \{0, 1, 2, \ldots, M\}$, where $M = \lfloor \frac{T}{h} \rfloor$ is specified. Additionally, the distributed output synchronization error is characterized by the term $\xi_{i,k}(t)$, which is formulated in the following manner

$$\xi_{i,k}(t) = \sum_{j=1}^{N} a_{ij}(\hat{y}_{j,k}(t) - y_{i,k}(t)) + b_i(y_d(t) - y_{i,k}(t)). \tag{9}$$

The pinning weight $b_i > 0$ if the leader informs node i, otherwise $b_i = 0$. The pinning gain matrix is $\mathcal{B} = \text{diag}\{b_1, \ldots, b_N\}$. The interaction topology is the augmented digraph $\overline{G} = \{\Lambda \cup \{0\}, \overline{\mathcal{E}}, \overline{\Theta}\}$ with a spanning tree.

Combining Equations (8) and (9) results in

$$\begin{aligned}\xi_{i,k}(t) &= \sum_{j=1}^{N} a_{i,j}(\hat{y}_{j,k}(t) - y_{i,k}(t)) + b_i(y_d(t) - y_{i,k}(t)) \\ &= \sum_{j=1}^{N} a_{i,j}(y_{j,k}(t) - y_{i,k}(t) - \beta_k \epsilon_{j,k}(t)) + b_i e_{i,k}(t) \\ &= \sum_{j=1}^{N} (a_{i,j} e_{i,k}(t) - a_{i,j} e_{j,k}(t)) + b_i e_{i,k}(t) - \beta_k \sum_{j=1}^{N} a_{i,j} \epsilon_{j,k}(t),\end{aligned} \tag{10}$$

where $e_{i,k}(t)$ is utilized to represent the output error associated with the k-th iteration. This term is formally established as the tracking deviation that exists between $y_d(t)$ and $y_{i,k}(t)$, the latter of which is produced throughout the real-time execution of the current control cycle

$$e_{i,k}(t) = y_d(t) - y_{i,k}(t).$$

Within the sampling interval $t \in [nh, nh + h)$, $\epsilon_{i,k}(t)$ remain as a specific constant.

The synthesis of the control input corresponding to the i-th node during the $(k+1)$-th iteration is formulated in the following manner

$$\begin{cases} u_{i,k+1}(t) = u_{i,k}(t) + \Gamma\xi_{i,k}(t), & t \in [nh, nh+h) \\ u_{i,k+1}(t) = u_{i,k+1}(nh), \end{cases}$$

where $\Gamma \in \mathbb{R}^{m\times p}$ denotes the learning gain matrix.

In the EEA-based event-triggered framework, k is the current iteration, and $\{k_l\}$ are the triggering iterations. The control law updates only at k_l, remaining constant for $k_l \le k < k_{l+1}$.

By integrating the aforementioned sampled-data framework with the event-triggered mechanism, the complete ET-EDSDILC protocol is ultimately formulated as follows

$$\begin{cases} u_{i,k+1}(t) = u_{i,k_l}(t) + \Gamma\xi_{i,k_l}(t) & k+1 = k_{l+1}, \\ u_{i,k}(nh) = u_{i,k_l}(nh) & k \in \{k_l, k_l+1, \ldots, k_{l+1}-1\}, \\ u_{i,k_l}(t) = u_{i,k_l}(nh) & t \in [nh, nh+h), \end{cases} \tag{11}$$

where $\xi_{i,k_l}(t)$ remains as a constant $\xi_{i,k_l}(nh)$ as $t \in [nh, nh+h)$.

For analytical convenience, the following notations are formally introduced

$$\begin{aligned} &u_{k_l}(t) = [u_{1,k_l}^T(t), u_{2,k_l}^T(t), ..., u_{N,k_l}^T(t)]^T; \xi_{k_l}(t) = [\xi_{1,k_l}^T(t), \xi_{2,k_l}^T(t), ..., \xi_{N,k_l}^T(t)]^T; \\ &r_{k_l}(t) = [r_{1,k_l}^T(t), r_{2,k_l}^T(t), ..., r_{N,k_l}^T(t)]^T; y_{k_l}(t) = [y_{1,k_l}^T(t), y_{2,k_l}^T(t), ..., y_{N,k_l}^T(t)]^T; \\ &\epsilon_{k_l}(t) = [\epsilon_{1,k_l}^T(t)\epsilon_{2,k_l}^T(t), ..., \epsilon_{N,k_l}^T(t)]^T; \end{aligned}$$

To reduce communication load, signals are transmitted at EEA-based event-triggered iterations, and the learning protocol is then formulated as follows.

$$u_{k_{l+1}}(t) = u_{k_l}(t) + (I_N \otimes \Gamma)\xi_{k_l}(t). \tag{12}$$

From Equation (10), as $t \in [nh, nh+h)$, it can be obtained that

$$\xi_{k_l}(t) = [(\mathcal{L}+\mathcal{B}) \otimes I_p]e_{k_l}(t) - \beta_{k_l}(\Theta \otimes I_p)\epsilon_{k_l}(t). \tag{13}$$

Substituting Equation (13) into Equation (12) yields the following result

$$u_{k_{l+1}}(t) = u_{k_l}(t) + [(\mathcal{L}+\mathcal{B}) \otimes \Gamma]e_{k_l}(t) - \beta_{k_l}(\Theta \otimes \Gamma)\epsilon_{k_l}(t), \tag{14}$$

where $e_{k_l}(t) = 1_N \otimes y_d(t) - y_{k_l}(t)$ represents the output consensus error under the EEA-based mechanism.

4.2. Design of Dynamic EEA-Based Event-Triggered Mechanism

Based on the definition of the individual output error $e_{i,k}(t)$, its compact vectorized representation is given by

$$e_k(t) = 1_N \otimes y_d(t) - y_k(t).$$

The collective output vector is defined as $y_k(t) = [y_{1,k}^{\mathrm{T}}(t), \ldots, y_{N,k}^{\mathrm{T}}(t)]^{\mathrm{T}}$. For further analytical tractability, the compact augmented state vector is likewise formulated as $x_k(t) = [x_{1,k}^{\mathrm{T}}(t), \ldots, x_{N,k}^{\mathrm{T}}(t)]^{\mathrm{T}}$.

In order to regulate the discrete update sequence within the iterative learning procedure, the iteration-axis error energy manifold is established as $R_k(t) = e_{k_l}(t) - e_k(t)$ for the interval $k \in \{k_l, k_l+1, \ldots, k_{l+1}-1\}$. The series of triggering iteration moments $\{k_l\}$

is systematically produced by a dynamic attenuation function $\chi(R_k(t))$, which quantifies whether the error dissipation along the iteration axis is sufficient. By taking the sampled-data control requirement $t = nh + h$ into account, the triggering law is stipulated in the following manner

$$\{k+1 = k_{l+1} \mid \chi(R_k(nh+h)) \geq 0\}.$$

The detailed formulation of the EEA-based triggering requirement for FOCPSs is delineated within the subsequent lemma.

Lemma 4. *Within the framework of the FOCPSs governed by the introduced ET-EDSDILC protocol, the EEA-based triggering mechanism $\chi(R_k(nh+h))$ is constructed as*

$$\chi(R_k(nh+h)) = \|R_k(nh+h)\|^2 - \frac{\eta\|e_k(nh+h)\|^2 - 2S_k^2(nh+h)}{2\left\|\frac{[(\mathcal{L}+\mathcal{B})\otimes CB\Gamma]}{\Xi(\alpha)}\frac{h^\alpha}{\alpha} + [(\mathcal{L}+\mathcal{B})\otimes D\Gamma]\right\|^2},$$

where the positive scalar $\eta \in (0,1]$ is utilized as a tunable variable to achieve a trade-off between stabilization and output synchronization velocity.

Remark 3. *The threshold parameter η balances communication efficiency and synchronization performance. Increasing η reduces communication frequency but may degrade tracking accuracy, whereas decreasing η improves synchronization accuracy at the expense of more transmissions.*

Additionally, the auxiliary operator $S_k(nh+h)$ is developed for the purpose of offsetting the influence of system nonlinearities and fractional-order dynamics, with its formulation presented below

$$\begin{aligned}
&S_k(nh+h) = \\
&\left\|\left[I - \left[\frac{[(\mathcal{L}+\mathcal{B})\otimes CB\Gamma]}{\Xi(\alpha)}\frac{h^\alpha}{\alpha} + [(\mathcal{L}+\mathcal{B})\otimes D\Gamma]\right]\right]e_k(nh+h)\right. \\
&-(I_N\otimes C)\Delta x_k(nh) - \frac{(I_N\otimes C)}{\Xi(\alpha)}\int_{nh}^{nh+h}(nh+h-s)^{\alpha-1}\Delta x_k(s)\,ds \\
&\left.-\left[\frac{\beta_{k_l}(\Theta\otimes CB\Gamma)}{\Xi(\alpha)}\frac{h^\alpha}{\alpha} + \beta_{k_l}(\Theta\otimes D\Gamma)\right]\epsilon_{k_l}(nh+h)\right\|,
\end{aligned}$$

with $\Delta x_k(t) = x_{k+1}(t) - x_k(t)$.

Proof. Using the Kronecker product, the FOCPSs (2) can be written compactly as the following manifold.

$$\begin{cases} \mathscr{D}_t^\alpha x_k(t) = (I_N\otimes A)x_k(t) + (I_N\otimes B)u_{k_l}(t), \\ y_k(t) = (I_N\otimes C)x_k(t) + (I_N\otimes D)u_{k_l}(t). \end{cases} \tag{15}$$

Based on the defined error $e_k(t)$, the output error recursion across iterations is given as follows

$$\begin{aligned} e_{k+1}(t) &= e_k(t) - y_{k+1}(t) + y_k(t) \\ &= e_k(t) - (I_N\otimes C)\Delta x_k(t) - (I_N\otimes D)\Delta u_{k_l}(t), \end{aligned} \tag{16}$$

with $\Delta u_{k_l}(t) = u_{k_{l+1}}(t) - u_{k_l}(t)$.

Based on the derivation in Equation (14), it can be obtained that

$$\Delta u_{k_l}(t) = [(\mathcal{L}+\mathcal{B})\otimes\Gamma]e_{k_l}(t) - \beta_{k_l}(\Theta\otimes\Gamma)\epsilon_{k_l}(t). \tag{17}$$

Upon the integration of the ET-EDSDILC protocol described in Equation (17) into the error dynamics defined by Equation (16), the evolution of error propagation can be characterized in the following manner

$$e_{k+1}(t) = e_k(t) - (I_N \otimes C)\Delta x_k(t) - [(\mathcal{L}+\mathcal{B}) \otimes D\Gamma]e_{k_l}(t) + \beta_{k_l}(\Theta \otimes D\Gamma)\epsilon_{k_l}(t). \tag{18}$$

Moreover, by implementing Definition 1 within the sampled-data duration $t \in [nh, nh+h)$ and considering the zero-order hold characteristic of the control command, the state evolution $\Delta x_k(t)$ is integrated across the sampling timeframe. Consequently, the integral formulation of the error dynamics is derived as follows

$$\begin{aligned} e_{k+1}(t) = e_k(t) &- (I_N \otimes C)\Delta x_k(nh) - \frac{(I_N \otimes CA)}{\Xi(\alpha)} \int_{nh}^{t} (t-s)^{\alpha-1} \Delta x_k(s)\, ds \\ &- \frac{(I_N \otimes CB)}{\Xi(\alpha)} \int_{nh}^{t} (t-s)^{\alpha-1} \Delta u_{k_l}(s)\, ds - [(\mathcal{L}+\mathcal{B}) \otimes D\Gamma]e_{k_l}(t) \\ &+ \beta_{k_l}(\Theta \otimes D\Gamma)\epsilon_{k_l}(t). \end{aligned} \tag{19}$$

From Equation (11), it is evident that the control input $u_{k_l}(t)$ remains constant throughout the sampling interval $t \in [nh, nh+h)$. Based on Equation (19), it follows that

$$\begin{aligned} e_{k+1}(t) = e_k(t) &- (I_N \otimes C)\Delta x_k(nh) - \frac{(I_N \otimes CA)}{\Xi(\alpha)} \int_{nh}^{t} (t-s)^{\alpha-1} \Delta x_k(s)\, ds \\ &- \frac{[(\mathcal{L}+\mathcal{B}) \otimes CB\Gamma]}{\Xi(\alpha)} \int_{nh}^{t} (t-s)^{\alpha-1}\, ds e_{k_l}(t) - [(\mathcal{L}+\mathcal{B}) \otimes D\Gamma]e_{k_l}(t) \\ &+ \frac{\beta_{k_l}(\Theta \otimes CB\Gamma)}{\Xi(\alpha)} \int_{nh}^{t} (t-s)^{\alpha-1}\, ds \epsilon_{k_l}(t) + \beta_{k_l}(\Theta \otimes D\Gamma)\epsilon_{k_l}(t). \end{aligned} \tag{20}$$

By collecting like terms and integrating the coefficients of $e_{k_l}(t)$ and $\epsilon_{k_l}(t)$, the following expression can be obtained that

$$\begin{aligned} e_{k+1}(t) = e_k(t) &- (I_N \otimes C)\Delta x_k(nh) - \frac{(I_N \otimes CA)}{\Xi(\alpha)} \int_{nh}^{t} (t-s)^{\alpha-1} \Delta x_k(s)\, ds \\ &- \left[\frac{[(\mathcal{L}+\mathcal{B}) \otimes CB\Gamma]}{\Xi(\alpha)} \frac{(t-nh)^{\alpha}}{\alpha} + [(\mathcal{L}+\mathcal{B}) \otimes D\Gamma] \right] e_{k_l}(t) \\ &- \left[\frac{\beta_{k_l}(\Theta \otimes CB\Gamma)}{\Xi(\alpha)} \frac{(t-nh)^{\alpha}}{\alpha} + \beta_{k_l}(\Theta \otimes D\Gamma) \right] \epsilon_{k_l}(t). \end{aligned} \tag{21}$$

To describe the sampling-induced deviation, define the measurement error as $R_k(t) = e_{k_l}(t) - e_k(t)$. Then, the sampled error can be decomposed as follows

$$e_{k_l}(t) = R_k(t) + e_k(t). \tag{22}$$

Substituting Equation (22) into Equation (21), it follows that

$$\begin{aligned} e_{k+1}(t) = e_k(t) &- (I_N \otimes C)\Delta x_k(nh) - \frac{(I_N \otimes CA)}{\Xi(\alpha)} \int_{nh}^{t} (t-s)^{\alpha-1} \Delta x_k(s)\, ds \\ &- \left[\frac{[(\mathcal{L}+\mathcal{B}) \otimes CB\Gamma]}{\Xi(\alpha)} \frac{(t-nh)^{\alpha}}{\alpha} + [(\mathcal{L}+\mathcal{B}) \otimes D\Gamma] \right] R_k(t) \\ &- \left[\frac{[(\mathcal{L}+\mathcal{B}) \otimes CB\Gamma]}{\Xi(\alpha)} \frac{(t-nh)^{\alpha}}{\alpha} + [(\mathcal{L}+\mathcal{B}) \otimes D\Gamma] \right] e_k(t) \\ &- \left[\frac{\beta_{k_l}(\Theta \otimes CB\Gamma)}{\Xi(\alpha)} \frac{(t-nh)^{\alpha}}{\alpha} + \beta_{k_l}(\Theta \otimes D\Gamma) \right] \epsilon_{k_l}(t). \end{aligned} \tag{23}$$

Utilizing the sampling moment $t = nh + h$, the resultant mathematical expression is established based on the derivation from Equation (23)

$$\begin{aligned} e_{k+1}(nh+h) &= e_k(nh+h) - (I_N \otimes C)\Delta x_k(nh) \\ &- \frac{(I_N \otimes CA)}{\Xi(\alpha)} \int_{nh}^{nh+h} (nh+h-s)^{\alpha-1} \Delta x_k(s)\, ds \\ &- \left[\frac{[(\mathcal{L}+\mathcal{B}) \otimes CB\Gamma]}{\Xi(\alpha)} \frac{h^\alpha}{\alpha} + [(\mathcal{L}+\mathcal{B}) \otimes D\Gamma] \right] R_k(nh+h) \\ &- \left[\frac{[(\mathcal{L}+\mathcal{B}) \otimes CB\Gamma]}{\Xi(\alpha)} \frac{h^\alpha}{\alpha} + [(\mathcal{L}+\mathcal{B}) \otimes D\Gamma] \right] e_k(nh+h) \\ &- \left[\frac{\beta_{k_l}(\Theta \otimes CB\Gamma)}{\Xi(\alpha)} \frac{h^\alpha}{\alpha} + \beta_{k_l}(\Theta \otimes D\Gamma) \right] \epsilon_{k_l}(nh+h). \end{aligned}$$

To regulate the transmission frequency and mitigate communication resource consumption, the EEA-based event-triggered function is defined as follows

$$M_{k+1}(t) = \|e_{k+1}(t)\|^2.$$

Furthermore, the auxiliary difference term $\Delta M_{k+1}(nh+h)$ is specifically defined as follows

$$\Delta M_{k+1}(nh+h) = M_{k+1}(nh+h) - \eta M_k(nh+h). \tag{24}$$

By substituting the derived expression of $e_{k+1}(nh+h)$ back into Equation (24), the following reformulated relation can be obtained

$$\begin{aligned} \Delta M_{k+1}(nh+h) &= \Bigg\| e_k(nh+h) - (I_N \otimes C)\Delta x_k(nh) \\ &- \frac{(I_N \otimes CA)}{\Xi(\alpha)} \int_{nh}^{nh+h} (nh+h-s)^{\alpha-1} \Delta x_k(s)\, ds \\ &- \left[\frac{[(\mathcal{L}+\mathcal{B}) \otimes CB\Gamma]}{\Xi(\alpha)} \frac{h^\alpha}{\alpha} + [(\mathcal{L}+\mathcal{B}) \otimes D\Gamma] \right] R_k(nh+h) \\ &- \left[\frac{[(\mathcal{L}+\mathcal{B}) \otimes CB\Gamma]}{\Xi(\alpha)} \frac{h^\alpha}{\alpha} + [(\mathcal{L}+\mathcal{B}) \otimes D\Gamma] \right] e_k(nh+h) \\ &- \left[\frac{\beta_{k_l}(\Theta \otimes CB\Gamma)}{\Xi(\alpha)} \frac{h^\alpha}{\alpha} + \beta_{k_l}(\Theta \otimes D\Gamma) \right] \epsilon_{k_l}(nh+h) \Bigg\|^2 \\ &- \eta \|e_k(nh+h)\|^2. \end{aligned} \tag{25}$$

Utilizing the Cauchy-Schwarz inequality, specifically in the elementary form $(a+b)^2 \leq 2a^2 + 2b^2$, to the expression in Equation (25), the subsequent analytical formulation is deduced

$$\begin{aligned} &\Delta M_{k+1}(nh+h) \\ &\leq 2 \left\| \frac{[(\mathcal{L}+\mathcal{B}) \otimes CB\Gamma]}{\Xi(\alpha)} \frac{h^\alpha}{\alpha} + [(\mathcal{L}+\mathcal{B}) \otimes D\Gamma] \right\|^2 \|R_k(nh+h)\|^2 \\ &+ 2 \left\| \left[I - \left[\frac{[(\mathcal{L}+\mathcal{B}) \otimes CB\Gamma]}{\Xi(\alpha)} \frac{h^\alpha}{\alpha} + [(\mathcal{L}+\mathcal{B}) \otimes D\Gamma] \right] \right] e_k(nh+h) \right. \\ &\quad - (I_N \otimes C)\Delta x_k(nh) - \frac{(I_N \otimes CA)}{\Xi(\alpha)} \int_{nh}^{nh+h} (nh+h-s)^{\alpha-1} \Delta x_k(s)\, ds \\ &\quad \left. - \left[\frac{\beta_{k_l}(\Theta \otimes CB\Gamma)}{\Xi(\alpha)} \frac{h^\alpha}{\alpha} + \beta_{k_l}(\Theta \otimes D\Gamma) \right] \epsilon_{k_l}(nh+h) \right\|^2 \\ &\quad - \eta \|e_k(nh+h)\|^2. \end{aligned} \tag{26}$$

Provided that the inequality $\Delta M_{k+1}(nh+h) < 0$ remains valid, it is ascertained that the execution of the triggering event will be suspended.

For the purpose of providing a rigorous description of the error dissipation within the FOCPSs, the auxiliary error operator $S_k(nh+h)$ is constructed in the following manner

$$\begin{aligned} &S_k(nh+h) = \\ &\Bigg\| \left[I - \left[\frac{[(\mathcal{L}+\mathcal{B}) \otimes CB\Gamma]}{\Xi(\alpha)} \frac{h^\alpha}{\alpha} + [(\mathcal{L}+\mathcal{B}) \otimes D\Gamma] \right] \right] e_k(nh+h) \\ &- (I_N \otimes C)\Delta x_k(nh) - \frac{(I_N \otimes CA)}{\Xi(\alpha)} \int_{nh}^{nh+h} (nh+h-s)^{\alpha-1} \Delta x_k(s)\, ds \\ &- \left[\frac{\beta_{k_l}(\Theta \otimes CB\Gamma)}{\Xi(\alpha)} \frac{h^\alpha}{\alpha} + \beta_{k_l}(\Theta \otimes D\Gamma) \right] \epsilon_{k_l}(nh+h) \Bigg\|. \end{aligned}$$

For the guarantee of monotonic convergence of the output synchronization error energy in the iteration domain, the inequality presented below needs to be satisfied

$$\|R_k(nh+h)\|^2 \geq \frac{\eta \|e_k(nh+h)\|^2 - 2S_k^2(nh+h)}{2\left\| \frac{[(\mathcal{L}+\mathcal{B}) \otimes CB\Gamma]}{\Xi(\alpha)} \frac{h^\alpha}{\alpha} + [(\mathcal{L}+\mathcal{B}) \otimes D\Gamma] \right\|^2}.$$

Under the EEA-based event-triggered scheme, the dynamic triggering function $\chi(R_k(nh+h))$ is derived and formulated as follows

$$\chi(R_k(nh+h)) = \|R_k(nh+h)\|^2 - \frac{\eta \|e_k(nh+h)\|^2 - 2S_k^2(nh+h)}{2\left\| \frac{[(\mathcal{L}+\mathcal{B}) \otimes CB\Gamma]}{\Xi(\alpha)} \frac{h^\alpha}{\alpha} + [(\mathcal{L}+\mathcal{B}) \otimes D\Gamma] \right\|^2}.$$

Consequently, the update of the ET-EDSDILC protocol is determined by the integrated triggering mechanism presented below

$$\{k+1 = k_{l+1} | \|e_k(nh+h)\| > \theta \quad \text{or} \quad \chi(R_k(nh+h)) \geq 0\}.$$

The ET-EDSDILC protocol re-triggers only when the error exceeds $\theta > 0$ or the error energy attenuation is insufficient, balancing communication savings and synchronization accuracy. □

5. Sufficient Conditions for Output Synchronization of FOCPSs

Theorem 1. *Consider the FOCPSs under the ET-EDSDILC protocol while satisfying Assumption 1. If the learning gain is designed to meet the following condition*

$$\begin{cases} \rho = \|I_{Np} - [(\mathcal{L}+\mathcal{B}) \otimes D\Gamma]\| < 1, \\ \frac{\tilde{\rho}}{\mathcal{K}} < 1, \end{cases} \tag{27}$$

As the number of iterations k_l and the number of samples M approach infinity,

$$\lim_{k_l \to \infty} \left\| y_{i,k}(t) - y_{j,k}(t) \right\| = 0, \quad \forall t \in [0, T]$$

will be achieved.

For all $i \in \Lambda$, the quantizers remain bounded throughout all iterations, provided that the aforementioned output synchronization conditions are satisfied.

$$\left\| \frac{y_{i,k_{l+1}} - \phi_{i,k_l}}{\beta_{k_l}} \right\|_\infty \leqslant \begin{cases} e^{\lambda T} \left(\frac{\tilde{\rho} \|e_0\|_\lambda}{\beta_0} + \mathcal{K}\varpi \right) + \frac{\|y_d\|_\infty}{\beta_0}, & k_l = 0, \\ e^{\lambda T} \left(\frac{\|e_0\|_\lambda}{\beta_0}(1+\tilde{\rho}) + \frac{\varpi \mathcal{K}}{\mathcal{K}-\tilde{\rho}} + \frac{\varpi}{\mathcal{K}-\tilde{\rho}} \right) + \frac{\sqrt{N}p}{2\mathcal{K}}, & k_l \geqslant 1, \end{cases}$$

the definitions of ϖ, $\tilde{\rho}$ are given in the proof.

Proof. Our theoretical achievements are derived through a two-step process. In the first step, the output synchronization of the tracking error is rigorously established. Subsequently, the quantized values within the encoder-decoder framework are shown to be bounded in the second step.

Part I: The compact form of the FOCPSs, which are entirely governed by iterative processes, can be formulated as follows

$$\begin{cases} \mathscr{D}_t^{\alpha} x_{k_l}(t) = (I_N \otimes A)x_{k_l}(t) + (I_N \otimes B)u_{k_l}(t), \\ y_{k_l}(t) = (I_N \otimes C)x_{k_l}(t) + (I_N \otimes D)u_{k_l}(t). \end{cases} \tag{28}$$

Within the sampling timeframe $t \in [nh, nh+h)$, the evolution of the error dynamics can be described through the application of Equation (14) in the manner below

$$\begin{aligned} e_{k_{l+1}}(t) &= e_{k_l}(t) - (I_N \otimes C)\Delta x_{k_l}(t) - (I_N \otimes D)\Delta u_{k_l}(t) \\ &= \left[I_{Np} - [(\mathcal{L}+\mathcal{B}) \otimes D\Gamma]\right] e_{k_l}(t) - (I_N \otimes C)\Delta x_{k_l}(t) \\ &\quad + \beta_{k_l}(\Theta \otimes D\Gamma)\epsilon_{k_l}(t). \end{aligned} \tag{29}$$

From Equation (29), applying the fractional integration rule in Lemma 3 with $t_0 = 0$ gives the continuous-time error state. To fit the sampled-data framework and retain the non-local memory, the horizon $[0, t]$ is divided into the historical interval $[0, nh)$ and the current interval $[nh, t]$. Thus, for $t \in [nh, nh+h)$, $\Delta x_{k_l}(t)$ can be written as

$$\begin{aligned} \Delta x_{k_l}(t) &= x_{k_{l+1}}(t) - x_{k_l}(t) \\ &= \Delta x_{k_l}(nh) + \frac{(I_N \otimes A)}{\Xi(\alpha)} \int_{nh}^{t} (t-s)^{\alpha-1} \Delta x_{k_l}(s)\, ds \\ &\quad + \frac{(I_N \otimes B)}{\Xi(\alpha)} \int_{nh}^{t} (t-s)^{\alpha-1} \Delta u_{k_l}(s)\, ds + \mathcal{H}_{k_l}(t, nh), \end{aligned} \tag{30}$$

where the historical memory term $\mathcal{H}_{k_l}(t, nh)$ over $[0, nh)$ is

$$\mathcal{H}_{k_l}(t, nh) = \int_0^{nh} \left[(t-s)^{\alpha-1} - (nh-s)^{\alpha-1}\right] \left[\frac{(I_N \otimes A)}{\Xi(\alpha)} \Delta x_{k_l}(s) + \frac{(I_N \otimes B)}{\Xi(\alpha)} \Delta u_{k_l}(s)\right] ds. \tag{31}$$

Taking norms in Equations (30) and (31) yields

$$\begin{aligned} \|\Delta x_{k_l}(t)\| &\le \|\Delta x_{k_l}(nh)\| + \frac{\|I_N \otimes A\|}{\Xi(\alpha)} \int_{nh}^{t} (t-s)^{\alpha-1} \|\Delta x_{k_l}(s)\|\, ds \\ &\quad + \frac{\|I_N \otimes B\|}{\Xi(\alpha)} \int_{nh}^{t} (t-s)^{\alpha-1} \|\Delta u_{k_l}(s)\|\, ds + \|\mathcal{H}_{k_l}(t, nh)\|, \end{aligned} \tag{32}$$

with

$$\begin{aligned} &\|\mathcal{H}_{k_l}(t, nh)\| \le \\ &\int_0^{nh} \left[(nh-s)^{\alpha-1} - (t-s)^{\alpha-1}\right] \left[\frac{\|I_N \otimes A\|}{\Xi(\alpha)} \|\Delta x_{k_l}(s)\| + \frac{\|I_N \otimes B\|}{\Xi(\alpha)} \|\Delta u_{k_l}(s)\|\right] ds. \end{aligned}$$

Due to the memory property of fractional-order calculus, consecutive sampling intervals are coupled. An interval-by-interval induction method is used to handle this non-local effect. The proof starts from the first interval with $n = 0$, then verifies the case $n = 1$, and finally extends the argument to any interval $n \in \{0, \ldots, M\}$.

Case 0: By Assumption 1, the initial state deviation satisfies $\Delta x_{k_l}(0) = 0$. From Equation (29), at $t = 0$, one has

$$e_{k_{l+1}}(0) = \left[I_{Np} - [(\mathcal{L} + \mathcal{B}) \otimes D\Gamma]\right] e_{k_l}(0) + \beta_{k_l}(\Theta \otimes D\Gamma)\epsilon_{k_l}(0). \tag{33}$$

Taking the λ-norm of Equation (33) gives

$$\|e_{k_{l+1}}(0)\|_\lambda \leq \left\|I_{Np} - [(\mathcal{L} + \mathcal{B}) \otimes D\Gamma]\right\| \|e_{k_l}(0)\|_\lambda + \beta_{k_l}\|\Theta \otimes D\Gamma\| \|\epsilon_{k_l}(0)\|_\lambda. \tag{34}$$

Since $\|\epsilon_{k_l}\|_\lambda \leq \|\epsilon_{k_l}\|_\infty \leq \frac{1}{2}\sqrt{Np}$ and $\lim\limits_{k_l \to \infty} \beta_{k_l} = 0$, the condition $\left\|I_{Np} - [(\mathcal{L} + \mathcal{B}) \otimes D\Gamma]\right\| < 1$ gives $\lim\limits_{k_l \to \infty} \|e_{k_l}(0)\|_\lambda = 0$.

Taking the norm of Equation (17) yields

$$\|\Delta u_{k_l}(t)\| \leq \|(\mathcal{L} + \mathcal{B}) \otimes \Gamma\| \|e_{k_l}(t)\| + \beta_{k_l}\|\Theta \otimes \Gamma\| \|\epsilon_{k_l}(t)\|. \tag{35}$$

Since $\Delta u_{k_l}(t) = \Delta u_{k_l}(0)$ is constant over $t \in [0, h)$, taking the λ-norm in Equation (35) gives

$$\|\Delta u_{k_l}(0)\|_\lambda \leq \|(\mathcal{L} + \mathcal{B}) \otimes \Gamma\| \|e_{k_l}(0)\|_\lambda + \beta_{k_l}\|\Theta \otimes \Gamma\| \|\epsilon_{k_l}(0)\|_\lambda. \tag{36}$$

Using $\lim\limits_{k_l \to \infty} \beta_{k_l} = 0$ and $\lim\limits_{k_l \to \infty} \|e_{k_l}(0)\|_\lambda = 0$, Equation (36) gives

$$\lim_{k_l \to \infty} \|\Delta u_{k_l}(0)\|_\lambda = 0.$$

For the first sampling interval, $\|\mathcal{H}_{k_l}(t, 0)\| = 0$. From Equation (32), it follows that

$$\begin{aligned}
\|\Delta x_{k_l}(t)\| &\leq \frac{\|I_N \otimes A\|}{\Xi(\alpha)} \int_0^t (t-s)^{\alpha-1} \|\Delta x_{k_l}(s)\|\, ds \\
&\quad + \frac{\|I_N \otimes B\|}{\Xi(\alpha)} \int_0^t (t-s)^{\alpha-1} \|\Delta u_{k_l}(s)\|\, ds \\
&\leq \frac{\|I_N \otimes A\|}{\Xi(\alpha)} \int_0^t (t-s)^{\alpha-1} \|\Delta x_{k_l}(s)\|\, ds \\
&\quad + \frac{\|I_N \otimes B\|}{\Xi(\alpha)} \int_0^t (t-s)^{\alpha-1} e^{\lambda s}\, ds \|\Delta u_{k_l}(0)\|_\lambda.
\end{aligned} \tag{37}$$

By Lemma 1, for any $\lambda > 0$, one has

$$\begin{aligned}
&\frac{dt^\alpha E_{1,1+\alpha}(\lambda t)}{dt} = t^{\alpha-1} E_{1,\alpha}(\lambda t) > 0, \\
&\frac{1}{\Xi(\alpha)} \int_0^t (t-s)^{\alpha-1} e^{\lambda s} ds = t^\alpha E_{1,1+\alpha}(\lambda t),
\end{aligned}$$

which shows that $\frac{1}{\Xi(\alpha)} \int_0^t (t-s)^{\alpha-1} e^{\lambda s} ds$ is increasing.

Introduce the auxiliary functions

$$\begin{aligned}
v(t-s) &= \frac{\|I_N \otimes A\|}{\Xi(\alpha)} (t-s)^{\alpha-1}, \\
w(s) &= \frac{\|I_N \otimes B\|}{\Xi(\alpha)} \int_0^t (t-s)^{\alpha-1} e^{\lambda s}\, ds \|\Delta u_{k_l}(0)\|_\lambda.
\end{aligned}$$

Since $\frac{dw(s)}{ds} > 0$, Lemma 2 gives

$$\|\Delta x_{k_l}(t)\| \leq \frac{\|I_N \otimes B\|}{\Xi(\alpha)} \int_0^t (t-s)^{\alpha-1} e^{\lambda s}\, ds \|\Delta u_{k_l}(0)\|_\lambda \exp\left(\frac{\|I_N \otimes A\| h^\alpha}{\Xi(\alpha+1)}\right). \tag{38}$$

By variable substitutions and extension of the upper integration limit, it can be obtained that

$$\int_0^t (t-s)^{\alpha-1} e^{\lambda s}\, ds \xrightarrow{t-s=w} \int_0^t w^{\alpha-1} e^{\lambda(t-w)}\, dw = e^{\lambda t} \int_0^t w^{\alpha-1} e^{-\lambda w}\, dw$$
$$\xrightarrow{\lambda w=s} \frac{e^{\lambda t}}{\lambda^{\alpha}} \int_0^{\lambda t} s^{\alpha-1} e^{-s}\, ds < \frac{e^{\lambda t}}{\lambda^{\alpha}} \int_0^{\lambda t} s^{\alpha-1} e^{-s}\, ds = \frac{e^{\lambda t}}{\lambda^{\alpha}} \Xi(\alpha). \tag{39}$$

Substituting Equation (39) into Equation (38) yields

$$\begin{aligned} \|\Delta x_{k_l}(t)\| &\le \frac{\|I_N \otimes B\| \gamma_1 e^{\lambda t}}{\lambda^{\alpha}} \|\Delta u_{k_l}(0)\|_{\lambda} \\ &\le \frac{\|I_N \otimes B\| \gamma_1 e^{\lambda h}}{\lambda^{\alpha}} \|\Delta u_{k_l}(0)\|_{\lambda}, \end{aligned} \tag{40}$$

with $\gamma_1 = \exp\left(\frac{\|I_N \otimes A\| h^{\alpha}}{\Xi(\alpha+1)}\right)$.

As $k_l \to \infty$, using $\lim_{k_l \to \infty} \|\Delta u_{k_l}(0)\|_{\lambda} = 0$, Equation (40) gives

$$\lim_{k_l \to \infty} \|\Delta x_{k_l}(t)\| = 0 \quad \forall t \in [0, h). \tag{41}$$

From the definition of $\|\mathcal{H}_{k_l}(t, nh)\|$, for $t \in [0, h)$, one can get

$$\|\mathcal{H}_{k_l}(t,h)\| = \int_0^h \left[(h-s)^{\alpha-1} - (t-s)^{\alpha-1}\right] \left[\frac{\|I_N \otimes A\|}{\Xi(\alpha)} \|\Delta x_{k_l}(s)\| + \frac{\|I_N \otimes B\|}{\Xi(\alpha)} \|\Delta u_{k_l}(s)\|\right] ds.$$

Since $\lim_{k_l \to \infty} \|\Delta u_{k_l}(t)\| \le \lim_{k_l \to \infty} \|\Delta u_{k_l}(0)\|_{\lambda} = 0$ and $\lim_{k_l \to \infty} \|\Delta x_{k_l}(t)\| = 0$, the above equation gives

$$\lim_{k_l \to \infty} \|\mathcal{H}_{k_l}(t,h)\| = 0. \tag{42}$$

Case 1: By the continuity of fractional-order state trajectories at sampling nodes, taking the left-hand limit as $t \to h^{-}$ gives

$$0 \le \lim_{k_l \to \infty} \|\Delta x_{k_l}(h)\| \le \lim_{k_l \to \infty} e^{\lambda h} \|\Delta x_{k_l}(t)\|_{\lambda} = 0, \tag{43}$$

which implies $\lim_{k_l \to \infty} \|\Delta x_{k_l}(h)\| = 0$ and $\lim_{k_l \to \infty} \|\Delta x_{k_l}(h)\|_{\lambda} = 0$.

At the sampling instant $t = h$, the error dynamics are

$$e_{k_{l+1}}(h) = \left[I_{Np} - [(\mathcal{L} + \mathcal{B}) \otimes D\Gamma]\right] e_{k_l}(h) + (I_N \otimes C) \Delta x_{k_l}(h) + \beta_{k_l} (\Theta \otimes D\Gamma) \epsilon_{k_l}(h). \tag{44}$$

Taking the λ-norm in Equation (44) and using norm inequalities has

$$\begin{aligned} \|e_{k_{l+1}}(h)\|_{\lambda} \le{}& \left\|I_{Np} - [(\mathcal{L} + \mathcal{B}) \otimes D\Gamma]\right\| \|e_{k_l}(h)\|_{\lambda} + \|I_N \otimes C\| \|\Delta x_{k_l}(h)\|_{\lambda} \\ &+ \beta_{k_l} \|\Theta \otimes D\Gamma\| \|\epsilon_{k_l}(h)\|_{\lambda}. \end{aligned} \tag{45}$$

Since $\|\epsilon_{k_l}\|_{\lambda} \le \|\epsilon_{k_l}\|_{\infty} \le \frac{1}{2}\sqrt{Np}$, $\lim_{k_l \to \infty} \beta_{k_l} = 0$, and $\lim_{k_l \to \infty} \|\Delta x_{k_l}(h)\|_{\lambda} = 0$, the condition $\left\|I_{Np} - [(\mathcal{L} + \mathcal{B}) \otimes D\Gamma]\right\| < 1$ guarantees $\lim_{k_l \to \infty} \|e_{k_l}(h)\|_{\lambda} = 0$.

Taking the norm of the control update protocol in Equation (17) at $t = h$ gives

$$\|\Delta u_{k_l}(h)\| \le \|(\mathcal{L} + \mathcal{B}) \otimes \Gamma\| \|e_{k_l}(h)\| + \beta_{k_l} \|\Theta \otimes \Gamma\| \|\epsilon_{k_l}(h)\|. \tag{46}$$

Since the control sequence is held constant over $t \in [h, 2h)$, one has $\Delta u_{k_l}(t) = \Delta u_{k_l}(h)$. Taking the λ-norm in Equation (46) yields

$$\|\Delta u_{k_l}(h)\|_\lambda \leq \|(\mathcal{L} + \mathcal{B}) \otimes \Gamma\| \|e_{k_l}(h)\|_\lambda + \beta_{k_l} \|\Theta \otimes \Gamma\| \|\epsilon_{k_l}(h)\|_\lambda. \tag{47}$$

The previous convergence results imply from Equation (47) that

$$\lim_{k_l \to \infty} \|\Delta u_{k_l}(h)\|_\lambda = 0.$$

For the second sampling window $t \in [h, 2h)$ with $n = 1$, Equation (32) can be rewritten as

$$\begin{aligned}
\|\Delta x_{k_l}(t)\| &\leq \|\Delta x_{k_l}(h)\| + \|\mathcal{H}_{k_l}(t,h)\| + \frac{\|I_N \otimes A\|}{\Xi(\alpha)} \int_h^t (t-s)^{\alpha-1} \|\Delta x_{k_l}(s)\| \, ds \\
&\quad + \frac{\|I_N \otimes B\|}{\Xi(\alpha)} \int_h^t (t-s)^{\alpha-1} \|\Delta u_{k_l}(s)\| \, ds \\
&\leq \|\Delta x_{k_l}(h)\| + \|\mathcal{H}_{k_l}(t,h)\| + \frac{\|I_N \otimes A\|}{\Xi(\alpha)} \int_h^t (t-s)^{\alpha-1} \|\Delta x_{k_l}(s)\| \, ds \\
&\quad + \frac{\|I_N \otimes B\|}{\Xi(\alpha)} \int_h^t (t-s)^{\alpha-1} e^{\lambda s} \, ds \|\Delta u_{k_l}(h)\|_\lambda.
\end{aligned} \tag{48}$$

For the convenience of subsequent analysis, the following auxiliary functions are introduced

$$\begin{aligned}
v(t-s) &= \frac{\|I_N \otimes A\|}{\Xi(\alpha)} (t-s)^{\alpha-1}, \\
w(s) &= \frac{\|I_N \otimes B\|}{\Xi(\alpha)} \int_h^t (t-s)^{\alpha-1} e^{\lambda s} \, ds \|\Delta u_{k_l}(h)\|_\lambda.
\end{aligned}$$

The strict monotonicity $\frac{dw(s)}{ds} > 0$ validates the application of Lemma 2, yielding the following upper bound

$$\begin{aligned}
\|\Delta x_{k_l}(t)\| &\leq \gamma_1 \|\Delta x_{k_l}(h)\| + \gamma_1 \|\mathcal{H}_{k_l}(t,h)\| \\
&\quad + \frac{\gamma_1 \|I_N \otimes B\|}{\Xi(\alpha)} \int_h^t (t-s)^{\alpha-1} e^{\lambda s} \, ds \|\Delta u_{k_l}(h)\|_\lambda.
\end{aligned} \tag{49}$$

The integral kernel is uniformly bounded as

$$\begin{aligned}
&\int_h^t (t-s)^{\alpha-1} e^{\lambda s} \, ds \overset{t-s=w}{=\!=\!=} \int_0^{t-h} w^{\alpha-1} e^{\lambda(t-w)} \, dw = e^{\lambda t} \int_0^{t-h} w^{\alpha-1} e^{-\lambda w} \, dw \\
&\overset{\lambda w = s}{=\!=\!=} \frac{e^{\lambda t}}{\lambda^\alpha} \int_0^{\lambda(t-h)} s^{\alpha-1} e^{-s} \, ds < \frac{e^{\lambda t}}{\lambda^\alpha} \int_0^{\lambda t} s^{\alpha-1} e^{-s} \, ds = \frac{e^{\lambda t}}{\lambda^\alpha} \Xi(\alpha).
\end{aligned} \tag{50}$$

Substituting this bound into Equation (49) has

$$\|\Delta x_{k_l}(t)\| \leq \gamma_1 \|\Delta x_{k_l}(h)\| + \gamma_1 \|\mathcal{H}_{k_l}(t,h)\| + \frac{\|I_N \otimes B\| \gamma_1 e^{2\lambda h}}{\lambda^\alpha} \|\Delta u_{k_l}(h)\|_\lambda. \tag{51}$$

Thus, as $k_l \to \infty$, using $\lim_{k_l \to \infty} \|\Delta x_{k_l}(h)\| = 0$, $\lim_{k_l \to \infty} \|\mathcal{H}_{k_l}(t,h)\| = 0$, and $\lim_{k_l \to \infty} \|\Delta u_{k_l}(h)\|_\lambda = 0$, one obtains

$$\lim_{k_l \to \infty} \|\Delta x_{k_l}(t)\| = 0 \quad \forall t \in [h, 2h). \tag{52}$$

By state continuity, $\lim_{k_l \to \infty} \|\Delta x_{k_l}(2h)\| = 0$ and $\lim_{k_l \to \infty} \|\Delta x_{k_l}(2h)\|_\lambda = 0$. For the next interval $t \in [2h, 3h)$ with $n = 2$, the memory term is

$$\begin{aligned}
&\|\mathcal{H}_{k_l}(t, 2h)\| = \\
&\int_0^{2h} \left[(2h-s)^{\alpha-1} - (t-s)^{\alpha-1} \right] \left[\frac{\|I_N \otimes A\|}{\Xi(\alpha)} \|\Delta x_{k_l}(s)\| + \frac{\|I_N \otimes B\|}{\Xi(\alpha)} \|\Delta u_{k_l}(s)\| \right] ds.
\end{aligned}$$

Using the uniform convergence of the state and control deviations over $\forall t \in [h, 2h)$ together with Case 0, the limit of the memory term satisfies

$$\lim_{k_l \to \infty} \|\mathcal{H}_{k_l}(t, 2h)\| = 0. \tag{53}$$

Repeating the interval-by-interval argument, suppose that $\lim_{k_l \to \infty} \|e_{k_l}(t)\|_\lambda = 0$ holds on the previous intervals, and that the state and control deviations uniformly converge to zero over $[0, nh)$. By continuity at sampling instants, the boundary condition at the n-th sampling instant satisfies

$$\lim_{k_l \to \infty} \|\Delta x_{k_l}(nh)\| = 0, \quad \lim_{k_l \to \infty} \|\Delta x_{k_l}(nh)\|_\lambda = 0. \tag{54}$$

The historical memory residual over $[0, nh)$ therefore vanishes for the current interval $t \in [nh, nh + h)$:

$$\lim_{k_l \to \infty} \|\mathcal{H}_{k_l}(t, nh)\| = 0. \tag{55}$$

The output synchronization over $t \in [nh, nh + h)$ is then analyzed.

Applying the λ-norm to Equation (29) at the sampling instant gives

$$\begin{aligned} \|e_{k_{l+1}}(nh)\|_\lambda \leq \left\| I_{Np} - [(\mathcal{L} + \mathcal{B}) \otimes D\Gamma] \right\| \|e_{k_l}(nh)\|_\lambda + \|I_N \otimes C\| \|\Delta x_{k_l}(nh)\|_\lambda \\ + \beta_{k_l} \|\Theta \otimes D\Gamma\| \|\epsilon_{k_l}(nh)\|_\lambda. \end{aligned} \tag{56}$$

Under the sufficient condition $\rho = \left\| I_{Np} - [(\mathcal{L} + \mathcal{B}) \otimes D\Gamma] \right\| < 1$, together with $\lim_{k_l \to \infty} \beta_{k_l} = 0$, $\lim_{k_l \to \infty} \|\Delta x_{k_l}(nh)\|_\lambda = 0$, and $\|\epsilon_{k_l}\|_\lambda \leq \|\epsilon_{k_l}\|_\infty \leq \frac{1}{2}\sqrt{Np}$, Equation (56) ensures $\lim_{k_l \to \infty} \|e_{k_l}(nh)\|_\lambda = 0$.

Taking the norm of Equation (17) at $t = nh$ gives

$$\|\Delta u_{k_l}(nh)\| \leq \|(\mathcal{L} + \mathcal{B}) \otimes \Gamma\| \|e_{k_l}(nh)\| + \beta_{k_l} \|\Theta \otimes \Gamma\| \|\epsilon_{k_l}(nh)\|. \tag{57}$$

Noting $\|e_{i,k_l}(t)\| = \|y_d(t) - y_{i,k_l}(t)\|$, one has

$$\lim_{k_l \to \infty} \|y_d(nh) - y_{i,k_l}(nh)\| = 0.$$

For any $i, j \in \Lambda$, the consensus error can be bounded by introducing $y_d(t)$ and using the triangle inequality:

$$\begin{aligned} \|y_{i,k_l}(nh) - y_{j,k_l}(nh)\| &= \|y_{i,k_l}(nh) - y_d(nh) - (y_{j,k_l}(nh) - y_d(nh))\| \\ &= \|e_{j,k_l}(nh) - e_{i,k_l}(mh)\| \leqslant \|e_{i,k_l}(nh)\| + \|e_{j,k_l}(nh)\|. \end{aligned} \tag{58}$$

Hence,

$$\lim_{k \to \infty} \left\| y_{i,k_l}(nh) - y_{j,k_l}(nh) \right\| = 0, \quad \forall i, j \in \Lambda.$$

The contraction mapping analysis in Part I gives exact zero-error convergence at the sampling instants $t = nh$. During inter-sample intervals, the control input is kept constant by zero-order hold. Since fractional-order state trajectories are continuous, the synchronization error remains bounded. As the number of sampling intervals M tends to infinity, the sampling period h tends to zero, and continuous-time full-track synchronization

is asymptotically recovered. Thus, the residual inter-sample errors are negligible.

As M approaches infinity, the control objective is theoretically achieved:

$$\lim_{k\to\infty}\left\|y_{i,k_l}(t)-y_{j,k_l}(t)\right\|=0,\quad \forall i,j\in\Lambda\quad t\in[0,T].$$

Part II: The uniform boundedness of the quantized values within the encoding-decoding framework is established as follows.

Since $\Delta x_{k_l}(0)=0$ by Assumption 1, applying Lemma 3 over the global horizon $[0,nh]$ to the compact FOCPS Equation (28) yields

$$\begin{aligned}\Delta x_{k_l}(nh)=&\frac{I_N\otimes A}{\Xi(\alpha)}\int_0^{nh}(nh-s)^{\alpha-1}\Delta x_{k_l}(s)\,ds\\&+\frac{I_N\otimes B}{\Xi(\alpha)}\int_0^{nh}(nh-s)^{\alpha-1}\Delta u_{k_l}(s)\,ds.\end{aligned}\tag{59}$$

Taking the norm of both sides of Equation (59) and recalling that $\Delta u_{k_l}(s)=\Delta u_{k_l}(n'h)$ is held constant for $s\in[n'h,(n'+1)h)$, $n'\in\{0,\dots,n-1\}$

$$\begin{aligned}\|\Delta x_{k_l}(nh)\|\le&\frac{\|I_N\otimes A\|}{\Xi(\alpha)}\int_0^{nh}(nh-s)^{\alpha-1}\|\Delta x_{k_l}(s)\|\,ds\\&+\frac{\|I_N\otimes B\|}{\Xi(\alpha)}\int_0^{nh}(nh-s)^{\alpha-1}e^{\lambda s}\,ds\cdot\sup_{n'\le n-1}\|\Delta u_{k_l}(n'h)\|_\lambda.\end{aligned}\tag{60}$$

By the same integral evaluation as in Equation (39)

$$\frac{1}{\Xi(\alpha)}\int_0^{nh}(nh-s)^{\alpha-1}e^{\lambda s}\,ds<\frac{e^{\lambda nh}}{\lambda^\alpha}.\tag{61}$$

Setting $v(nh-s)=\frac{\|I_N\otimes A\|}{\Xi(\alpha)}(nh-s)^{\alpha-1}$ and applying Lemma 2 to Equation (60) together with Equation (61) gives

$$\|\Delta x_{k_l}(nh)\|\le\frac{\|I_N\otimes B\|\,\gamma_n\,e^{\lambda nh}}{\lambda^\alpha}\sup_{n'\le n-1}\|\Delta u_{k_l}(n'h)\|_\lambda,\tag{62}$$

where $\gamma_n=\exp\left(\frac{\|I_N\otimes A\|T^\alpha}{\Xi(\alpha+1)}\right)$. Taking the λ-norm of both sides of Equation (62) and noting $e^{-\lambda nh}\le 1$ yields

$$\|\Delta x_{k_l}(nh)\|_\lambda\le\frac{\|I_N\otimes B\|\,\gamma_n}{\lambda^\alpha}\sup_{n'\le n-1}\|\Delta u_{k_l}(n'h)\|_\lambda.\tag{63}$$

From Equation (57), $\|\Delta u_{k_l}(n'h)\|_\lambda$ is bounded as

$$\|\Delta u_{k_l}(n'h)\|_\lambda\le\|(\mathcal{L}+\mathcal{B})\otimes\Gamma\|\,\|e_{k_l}(n'h)\|_\lambda+\beta_{k_l}\|\Theta\otimes\Gamma\|\,\|\epsilon_{k_l}(n'h)\|_\lambda.\tag{64}$$

Substituting Equation (64) into Equation (63) and denoting $\varsigma=\|I_N\otimes B\|\,\gamma_n\,\|(\mathcal{L}+\mathcal{B})\otimes\Gamma\|$, $\partial=\|I_N\otimes B\|\,\gamma_n\,\|\Theta\otimes\Gamma\|$

$$\|\Delta x_{k_l}(nh)\|_\lambda\le\frac{\varsigma}{\lambda^\alpha}\sup_{n'\le n-1}\|e_{k_l}(n'h)\|_\lambda+\frac{\beta_{k_l}\partial}{\lambda^\alpha}\sup_{n'\le n-1}\|\epsilon_{k_l}(n'h)\|_\lambda.\tag{65}$$

By the fundamental definition of the global λ-norm, any pointwise evaluation over the horizon $[0,T]$ is strictly bounded by its supremum, which implies that $\sup_{n'\le n-1}\|e_{k_l}(n'h)\|_\lambda\le\|e_{k_l}\|_\lambda$ and $\|e_{k_l}(nh)\|_\lambda\le\|e_{k_l}\|_\lambda$. Thus, Equation (65) can be uniformly bounded as

$$\|\Delta x_{k_l}(nh)\|_\lambda \leq \frac{\varsigma}{\lambda^\alpha}\|e_{k_l}\|_\lambda + \frac{\beta_{k_l}\partial\sqrt{Np}}{2\lambda^\alpha}. \tag{66}$$

Substituting Equation (66) into Equation (56) yields

$$\begin{aligned}\|e_{k_{l+1}}(nh)\|_\lambda \leq &\left(\rho + \frac{\|I_N \otimes C\|\varsigma}{\lambda^\alpha}\right)\|e_{k_l}(nh)\|_\lambda \\ &+ \beta_{k_l}\left(\frac{\|I_N \otimes C\|\partial}{\lambda^\alpha} + \|\Theta \otimes D\Gamma\|\right)\|\epsilon_{k_l}(nh)\|_\lambda.\end{aligned} \tag{67}$$

Defining $\tilde{\rho} = \rho + \frac{\|I_N \otimes C\|\varsigma}{\lambda^\alpha}$ and $\tilde{\partial} = \frac{\|I_N \otimes C\|\partial}{\lambda^\alpha} + \|\Theta \otimes D\Gamma\|$, and letting $\varpi = \frac{\tilde{\partial}\sqrt{Np}}{2}$, Equation (67) reduces to

$$\|e_{k_{l+1}}(nh)\|_\lambda \leq \tilde{\rho}\,\|e_{k_l}(nh)\|_\lambda + \beta_{k_l}\varpi. \tag{68}$$

Since $\rho < 1$, a sufficiently large λ can always be chosen such that $\tilde{\rho} < 1$ and $\tilde{\rho}/\mathcal{K} < 1$. Applying Equation (68) recursively gives

$$\|e_{k_{l+1}}\|_\lambda \leq \tilde{\rho}^{k_l+1}\|e_0\|_\lambda + \beta_0\varpi\sum_{r=0}^{k_l}\tilde{\rho}^r\mathcal{K}^{k_l-r}, \tag{69}$$

Furthermore, it can be obtained that

$$\|e_{k_{l+1}}\|_\infty \leq e^{\lambda T}\left(\tilde{\rho}^{k_l+1}\|e_0\|_\lambda + \beta_0\varpi\sum_{r=0}^{k_l}\tilde{\rho}^r\mathcal{K}^{k_l-r}\right). \tag{70}$$

Case 0: For the i-th agent at the initial triggering instant $k_l = 0$

$$\begin{aligned}\left\|\frac{y_{i,1}-\phi_{i,0}}{\beta_0}\right\|_\infty \leq \left\|\frac{y_{i,1}}{\beta_0}\right\|_\infty &\leq \frac{\|e_{i,1}\|_\infty + \|y_d\|_\infty}{\beta_0} \leq \frac{\|e_1\|_\infty + \|y_d\|_\infty}{\beta_0} \\ &\leq e^{\lambda T}\left(\frac{\tilde{\rho}\|e_0\|_\lambda}{\beta_0} + \mathcal{K}\varpi\right) + \frac{\|y_d\|_\infty}{\beta_0}.\end{aligned} \tag{71}$$

General case: Invoking Equation (7) and the triangle inequality for $k_l \geq 1$

$$\begin{aligned}&\left\|\frac{y_{i,k_l+1}-\phi_{i,k_l}}{\beta_{k_l}}\right\|_\infty \leq \frac{\|e_{k_l+1}\|_\infty + \|e_{k_l}\|_\infty}{\mathcal{K}^{k_l}\beta_0} + \frac{\|\epsilon_{k_l}\|_\infty}{\mathcal{K}} \\ &\leq e^{\lambda T}\left(\frac{\|e_0\|_\lambda}{\beta_0}(1+\tilde{\rho})\left(\frac{\tilde{\rho}}{\mathcal{K}}\right)^{k_l} + \varpi\sum_{r=0}^{k_l}\left(\frac{\tilde{\rho}}{\mathcal{K}}\right)^r + \frac{\varpi}{\mathcal{K}}\sum_{r=0}^{k_l-1}\left(\frac{\tilde{\rho}}{\mathcal{K}}\right)^r\right) + \frac{\sqrt{Np}}{2\mathcal{K}}.\end{aligned} \tag{72}$$

Since $\tilde{\rho}/\mathcal{K} < 1$, the geometric series converge and $(\tilde{\rho}/\mathcal{K})^{k_l}$ is uniformly bounded for all $k_l \geq 0$, yielding the following uniform upper bound for all $k_l \geq 1$

$$\left\|\frac{y_{i,k_l+1}-\phi_{i,k_l}}{\beta_{k_l}}\right\|_\infty \leq e^{\lambda T}\left(\frac{(1+\tilde{\rho})\|e_0\|_\lambda}{\beta_0} + \frac{\varpi\mathcal{K}}{\mathcal{K}-\tilde{\rho}} + \frac{\varpi}{\mathcal{K}-\tilde{\rho}}\right) + \frac{\sqrt{Np}}{2\mathcal{K}}. \tag{73}$$

The right-hand side of Equation (73) constitutes a finite constant independent of the iteration index k_l, which confirms that the argument of the uniform quantizer remains uniformly bounded across all triggering iterations under the proposed ET-EDSDILC protocol. The proof is thus completed. □

6. Numerical Simulation

In this section, a representative numerical example is provided to demonstrate the efficacy and finite-time output synchronization properties of the proposed ET-EDSDILC protocol.

The specific parameters are as follows $t \in [0,2], \alpha = 0.85$. Event-triggered parameters $\eta = 0.8, \theta = 0.2$. The initial parameters β_0 of the scaling sequence are defined as $\beta_0 = 1$, and the scaling factor is defined as $\mathcal{K} = 0.95$. The main matrices of FOCPSs are chosen as

$$A = \begin{bmatrix} -0.15 & 0 & 0.20 & 0 \\ 0 & -0.20 & 0 & 0.25 \\ 0 & 0 & -0.25 & 0 \\ 0 & 0 & 0 & -0.10 \end{bmatrix},$$

$B = \mathrm{diag}\{0.9, 0.9, 0.9, 0.9\}$, $C = \mathrm{diag}\{1,1,1,1\}$, $D = \mathrm{diag}\{1,1,1,1\}$. The total number of iterations k is set to 150.

Their desired trajectories are selected as $y_{d1}(t) = 40(1-t)\cos(10\pi t)$, $y_{d2}(t) = 40(1-t)\sin(10\pi t)$, $y_{d3}(t) = 30\sin(1.5\pi t)(t+0.5)$, $y_{d4}(t) = 30\cos(\pi t + \frac{\pi}{4})(1.2 - 16t^2(1-t)^2)$, and

$$y_d(t) = [y_{d1}(t), y_{d2}(t), y_{d3}(t), y_{d4}(t)]^T.$$

The fixed communication topology between nodes of FOCPSs is shown in Figure 2. The virtual leader is represented as number 0; it means only the second and forth agent can receive the desired states. The Laplacian matrix is as follows

$$\mathcal{L} = \begin{bmatrix} 1 & -1 & 0 & 0 \\ 0 & 1 & -1 & 0 \\ -1 & 0 & 1 & 0 \\ 0 & -1 & 0 & 1 \end{bmatrix}, \mathcal{B} = \begin{bmatrix} 0 & 0 & 0 & 0 \\ 0 & 1 & 0 & 0 \\ 0 & 0 & 0 & 0 \\ 0 & 0 & 0 & 1 \end{bmatrix}.$$

According to the Theorem 1, the gain matrix $\Gamma = \mathrm{diag}\{0.62, 0.55, 0.48, 0.61\}$ is chosen, it can be computed that $\rho = \left\| I_{Np} - [(\mathcal{L} + \mathcal{B}) \otimes D\Gamma] \right\| = 0.7686 < 1$, which means that the Theorem 1 is satisfied.

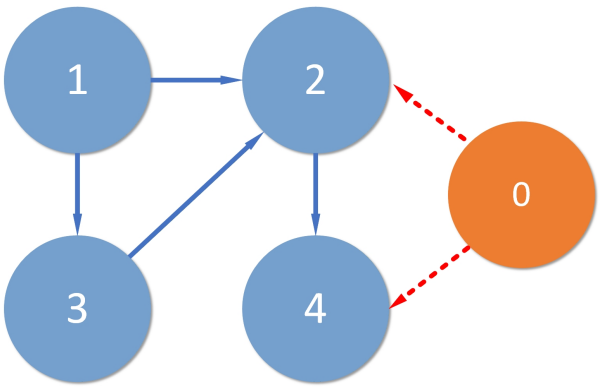


Figure 2. Fixed communication topology between FOCPSs.

The temporal evolution of the system output states, denoted by $y_1(t), y_2(t), y_3(t)$, and $y_4(t)$, over the predefined time horizon is illustrated in the graphical representations provided in Figures 3–10. It can be observed that as the iteration count is incrementally increased, the trajectories associated with all four FOCPS units are gradually steered toward a relatively unified and stable manifold. In particular, the chaotic oscillations and transient instabilities that are evident during the third iteration are progressively mitigated through the iterative refinement process. By the time the 50th iteration is reached, a relatively high degree of output synchronization is achieved among the respective FOCPS, indicating a

noticeable reduction in the variance of the state trajectories. This observed phenomenon suggests that, through the implementation of the proposed ET-EDSDILC protocol, the output synchronization errors can be effectively attenuated, and the desired tracking performance can be achieved within a finite iterative sequence, even in the presence of communication constraints.

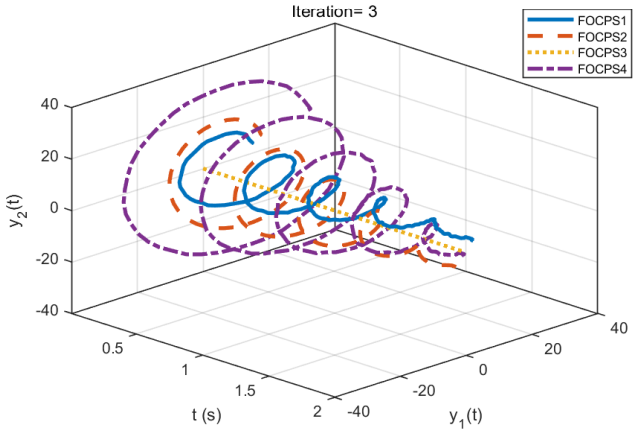


Figure 3. The output $y_1(t), y_2(t)$ in the three-dimensional space when $k_l = 3$.

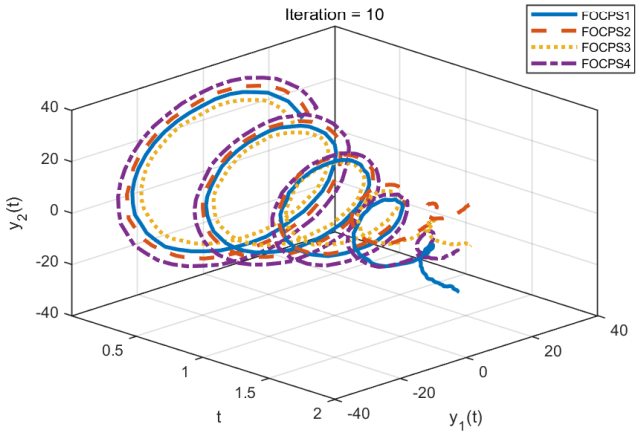


Figure 4. The output $y_1(t), y_2(t)$ in the three-dimensional space when $k_l = 10$.

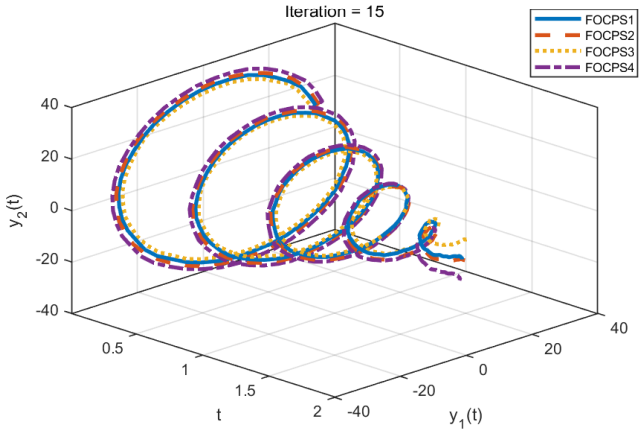


Figure 5. The output $y_1(t), y_2(t)$ in the three-dimensional space when $k_l = 15$.

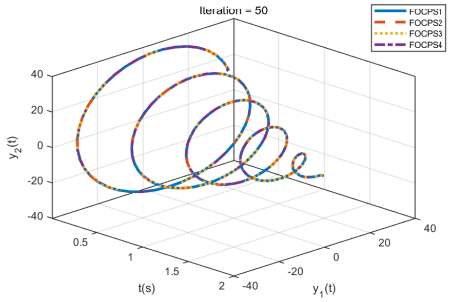


Figure 6. The output $y_1(t), y_2(t)$ in the three-dimensional space when $k_l = 50$.

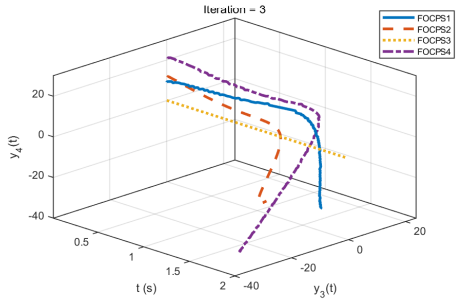


Figure 7. The output $y_3(t), y_4(t)$ in the three-dimensional space when $k_l = 3$.

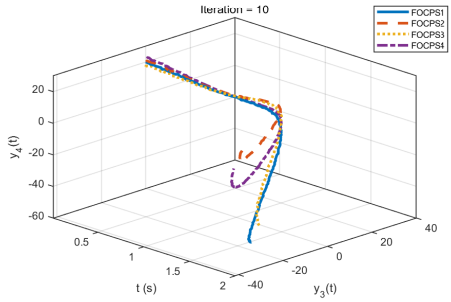


Figure 8. The output $y_3(t), y_4(t)$ in the three-dimensional space when $k_l = 10$.

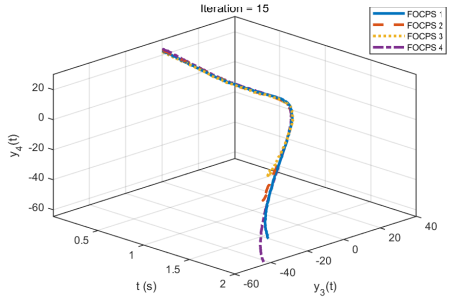


Figure 9. The output $y_3(t), y_4(t)$ in the three-dimensional space when $k_l = 15$.

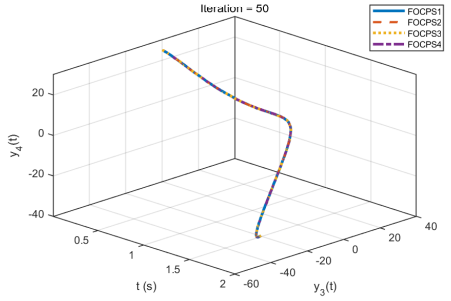


Figure 10. The output $y_3(t), y_4(t)$ in the three-dimensional space when $k_l = 50$.

The evolutionary performance and output synchronization characteristics of the proposed ET-EDSDILC protocol are illustrated in Figures 11–14. It is shown that both the individual output responses of the FOCPSs and the multifaceted state deviations are gradually steered toward the desired reference trajectories as the iteration index k_l progresses. Through the application of this iterative learning mechanism, output synchronization among the multiple FOCPS agents can be achieved, allowing the tracking objective to be approximately fulfilled across the temporal horizon. Furthermore, it can be observed that the residual output errors are progressively suppressed, thereby demonstrating the effectiveness of the control law under communication constraints inherent in the sampled-data environment.

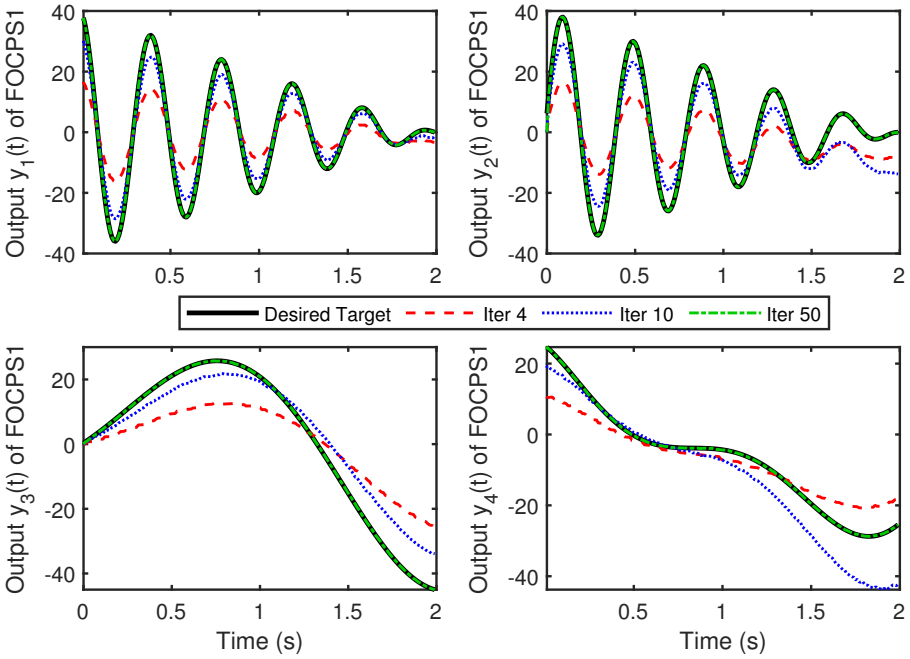


Figure 11. The output $y_1(t)-y_4(t)$ synchronization trajectory of FOCPS1.

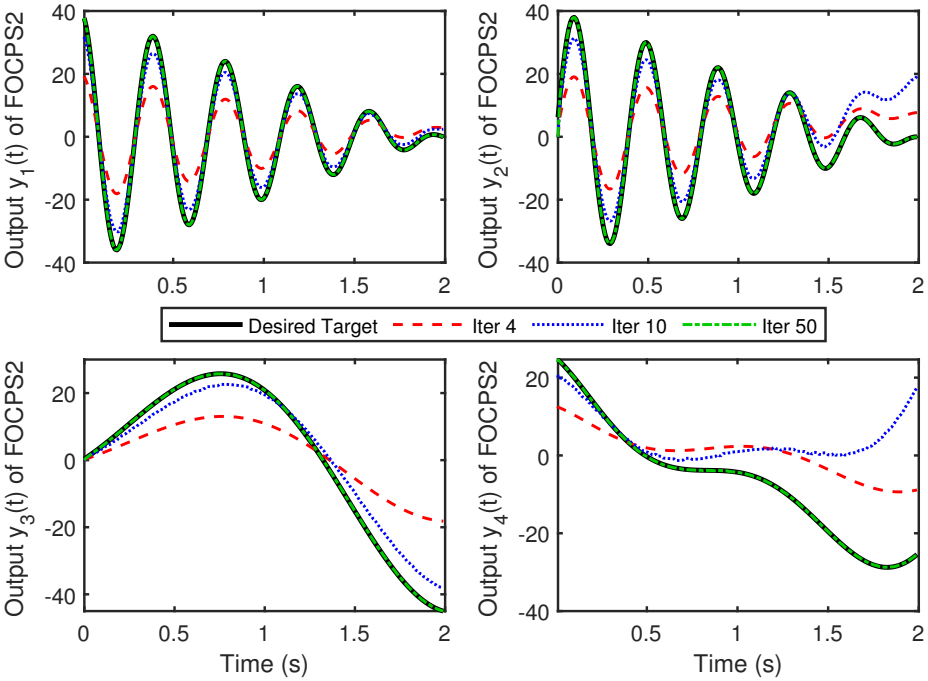


Figure 12. The output $y_1(t)-y_4(t)$ synchronization trajectory of FOCPS2.

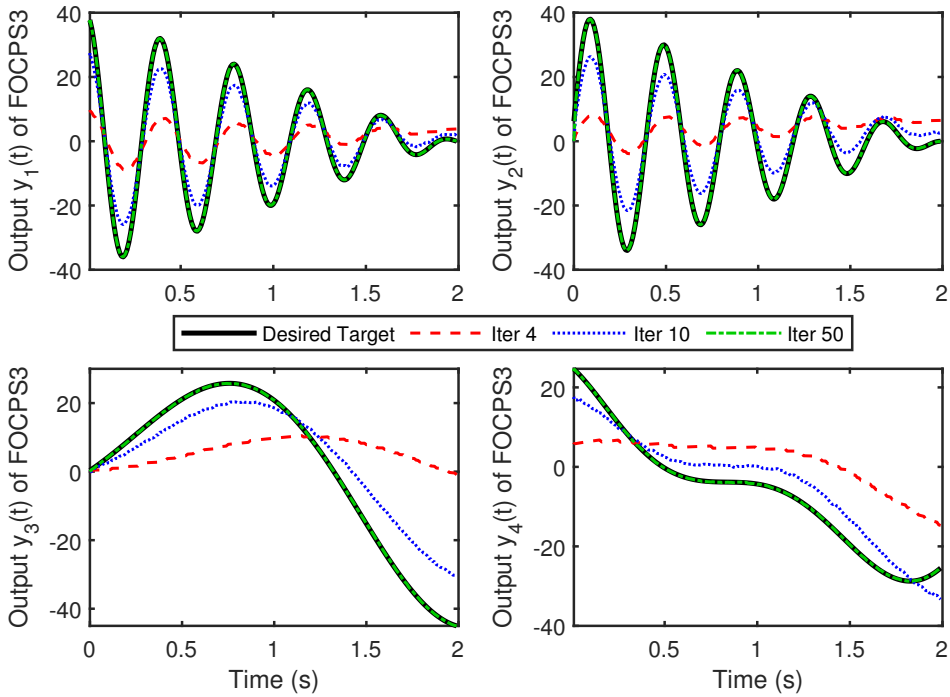


Figure 13. The output $y_1(t) - y_4(t)$ synchronization trajectory of FOCPS3.

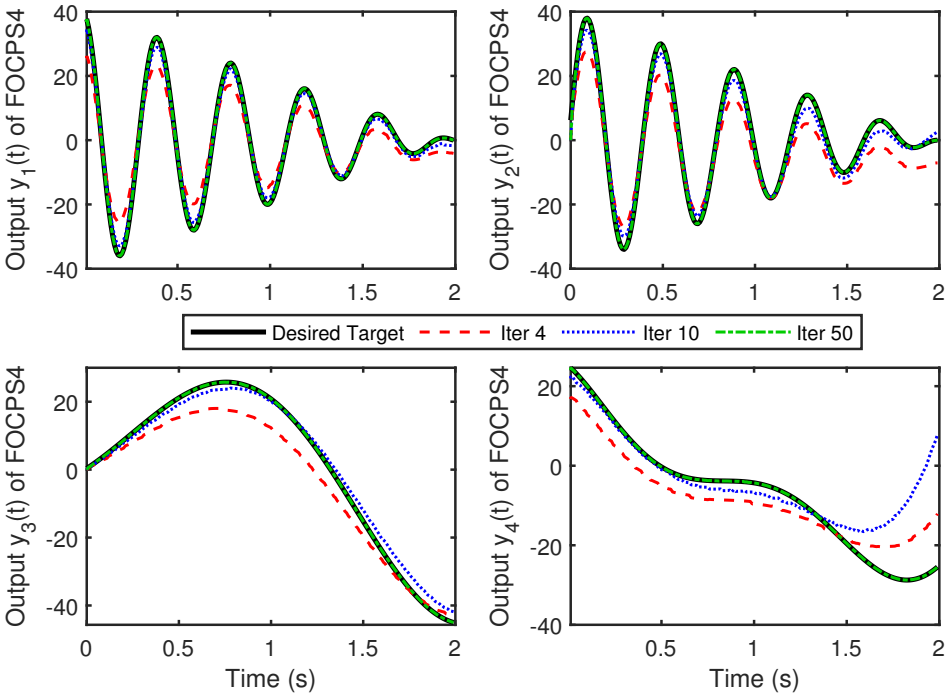


Figure 14. The output $y_1(t) - y_4(t)$ synchronization trajectory of FOCPS4.

Regarding the numerical results, the event-trigger counts of FOCPS 1 to FOCPS 4 are shown in Figures 15–18. The trigger frequencies vary with the iteration process under the proposed ET-EDSDILC law. Higher trigger rates appear in the early iterations, while the number of triggering events generally decreases as the iteration index k_l increases, indicating a reduction in communication updates. As reported in Table 1, the transmission rates of FOCPS 1 to FOCPS 4 are 72.11%, 69.47%, 71.99%, and 70.98%, respectively. These results suggest that, in the tested example, the proposed scheme can reduce part of the communication load while preserving acceptable output synchronization performance.

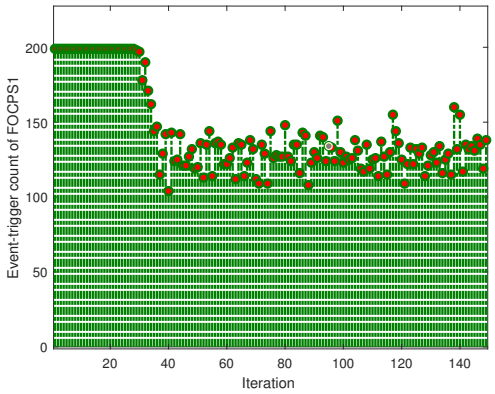


Figure 15. The number of trigger occurrences of FOCPS1.

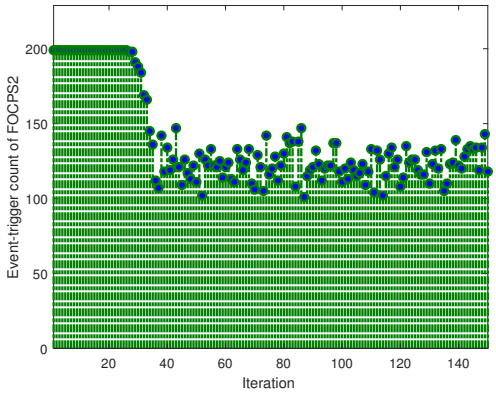


Figure 16. The number of trigger occurrences of FOCPS2.

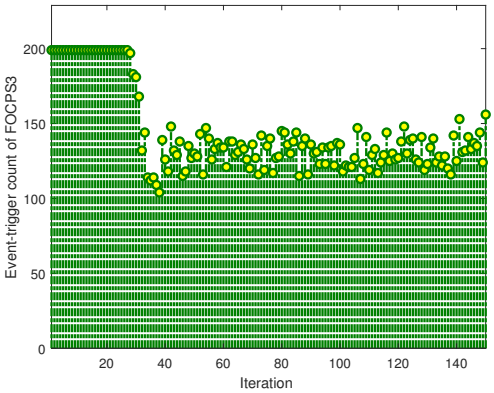


Figure 17. The number of trigger occurrences of FOCPS3.

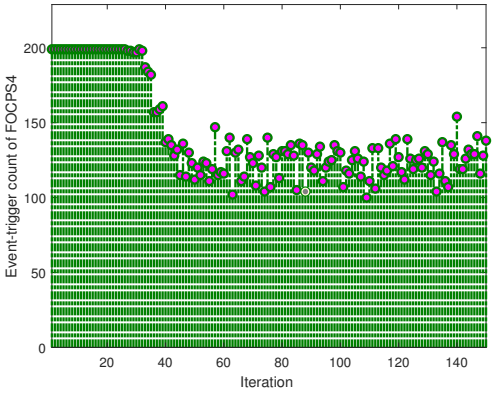


Figure 18. The number of trigger occurrences of FOCPS4.

Table 1. Total number of triggering times of each FOCPS.

	Actual Triggered Times	Maximum Triggered Times	Data Transmission
FOCPS1	21,634	30,000	72.11%
FOCPS2	20,846	30,000	69.47%
FOCPS3	21,596	30,000	71.99%
FOCPS4	21,295	30,000	70.98%

Remark 4. *The 100% triggering baseline sends data at every sample, totaling 30,000 transmissions per FOCPS. Achieving 70% transmission rates avoids 30% of overhead, saving communication resources in fractional-order iterative learning control systems while keeping tracking performance acceptable.*

Taking the four states of FOCPS 1 as a representative example, Figures 19–22 present the evolution of the encoder output $s(t)$ at different iterations. At the 5th iteration, the encoder outputs contain relatively large fluctuations and dense pulses, reflecting more frequent signal adjustments during the early learning stage. When the iteration index k_l increases to 20 and 100, both the signal amplitude and pulse density are reduced. This change indicates that the encoding process becomes less intensive as the tracking deviation decreases, which is consistent with the expected behavior of the proposed learning mechanism under quantized communication.

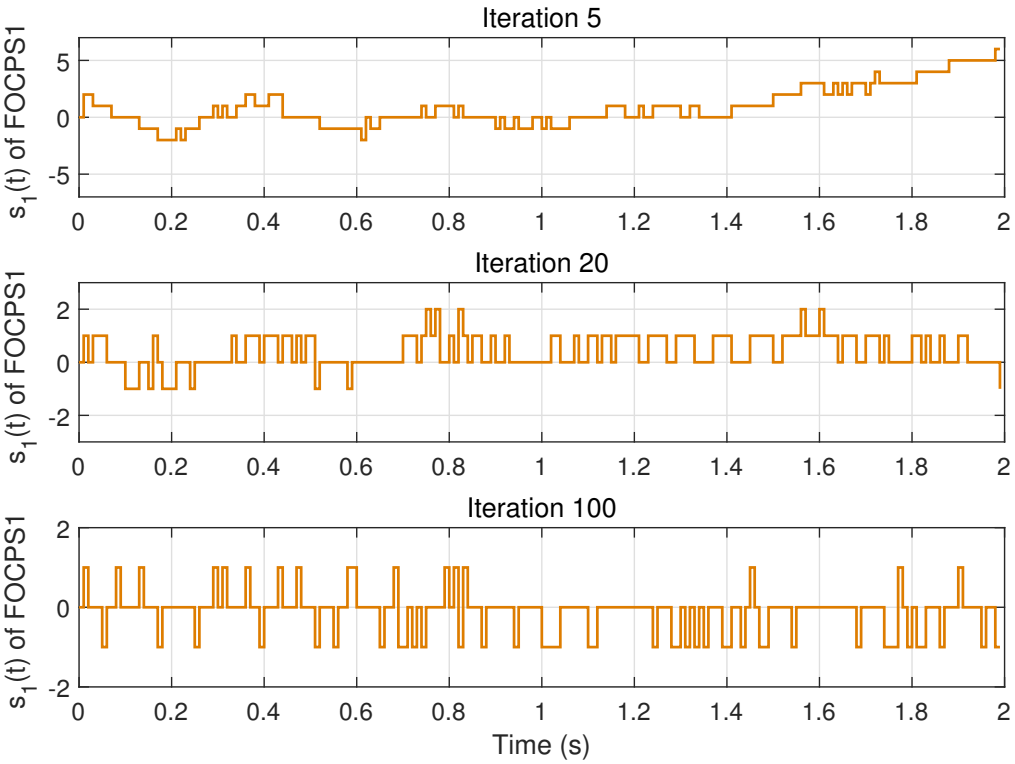


Figure 19. Evolution of the encoder output $s_1(t)$ of FOCPS1 with increasing iterations.

By the 100th iteration, the encoder output $s(t)$ mainly contains sparse and low-amplitude signals, suggesting that the tracking deviation has been reduced to a relatively small level. This trend indicates that the demand for quantization and encoding updates decreases as the iterative learning process proceeds. In the tested example, the proposed encoding–decoding mechanism helps reduce redundant data transmission while maintaining acceptable tracking performance.

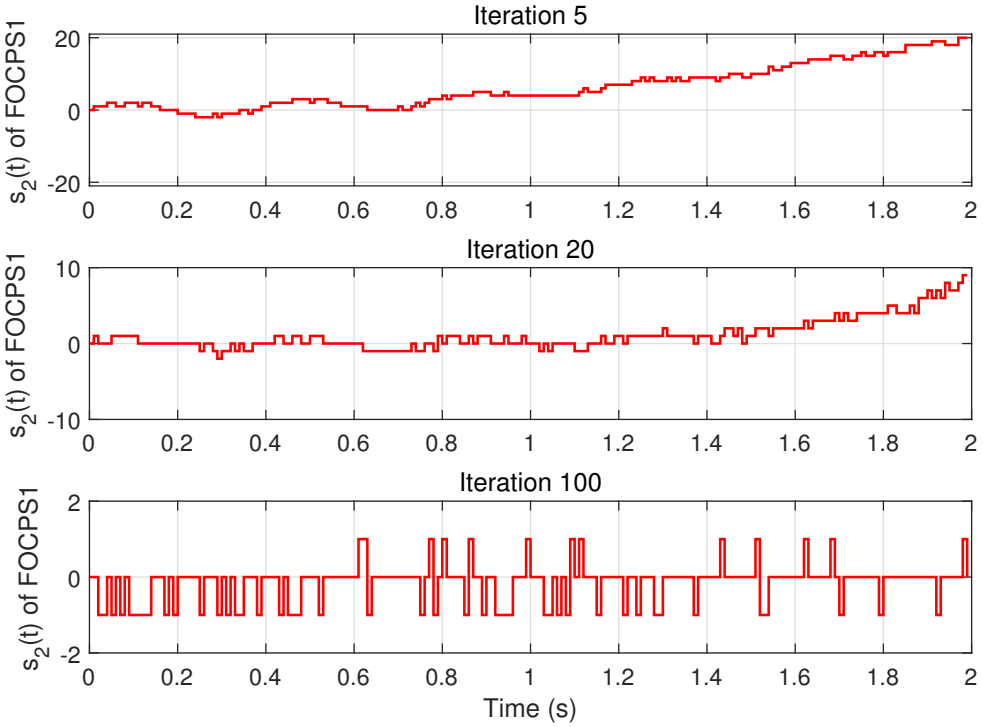


Figure 20. Evolution of the encoder output $s_2(t)$ of FOCPS1 with increasing iterations.

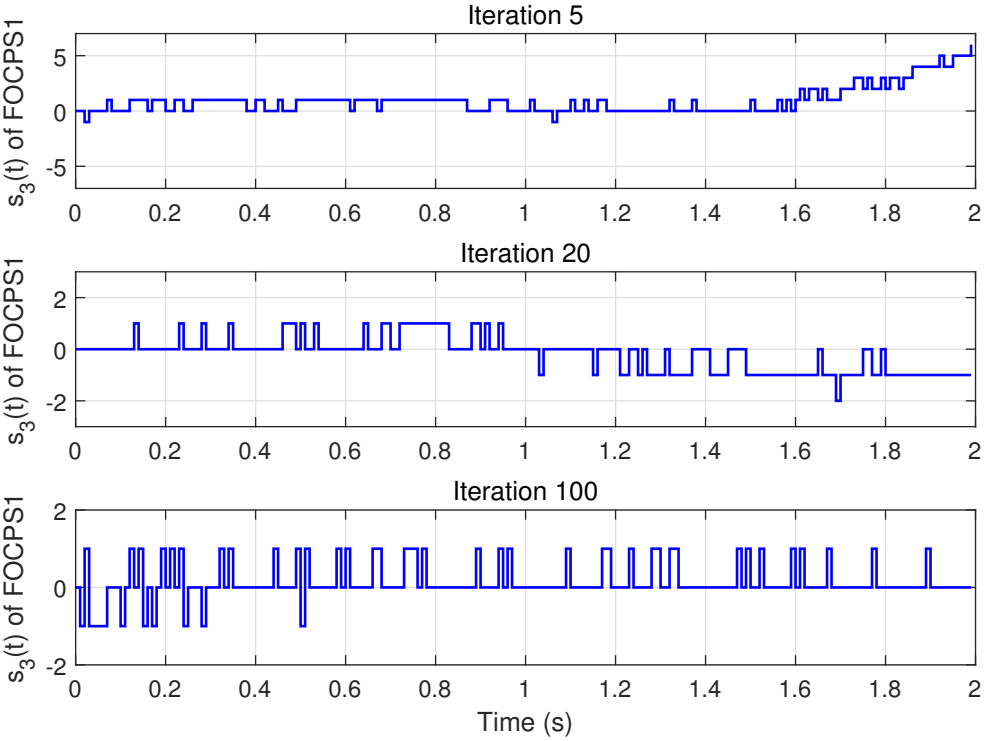


Figure 21. Evolution of the encoder output $s_3(t)$ of FOCPS1 with increasing iterations.

The evolution of the maximum distributed output synchronization errors, denoted as $\xi_{\max,i}$ $(i = 1, 2, 3, 4)$, for the four systems FOCPS 1 through FOCPS 4 is illustrated in Figures 23–26. It is observed that the trajectories of the maximum error components exhibit a consistent and monotonic decreasing trend over the course of 150 iterations. As the iteration index increases, the distributed synchronization errors $\xi_{\max,i}$ for all FOCPSs effectively converge toward a sufficiently small neighborhood of zero.

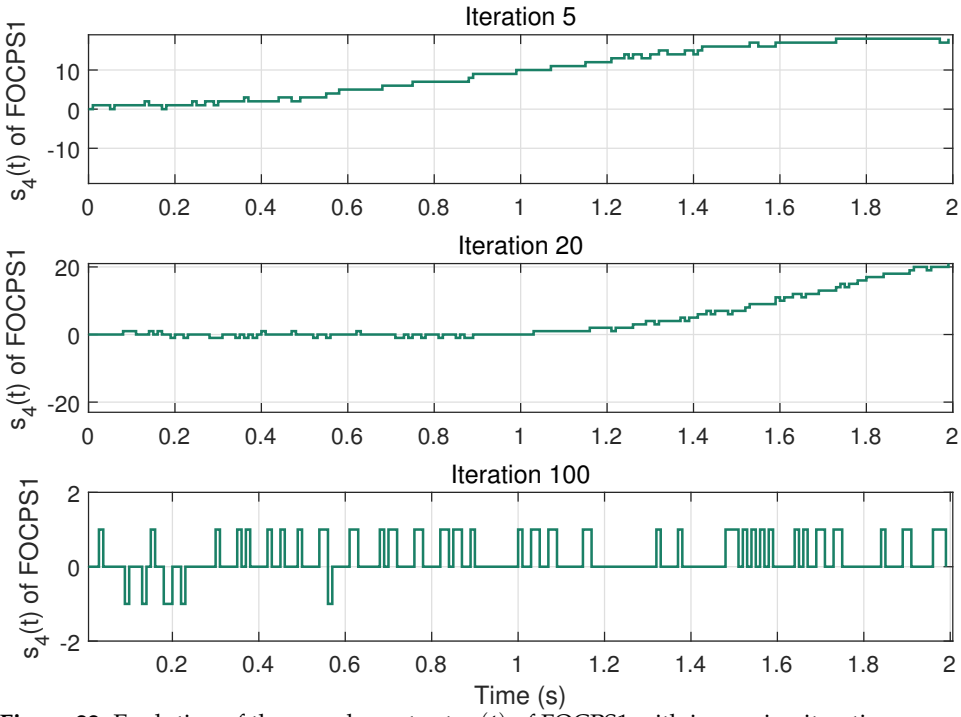


Figure 22. Evolution of the encoder output $s_4(t)$ of FOCPS1 with increasing iterations.

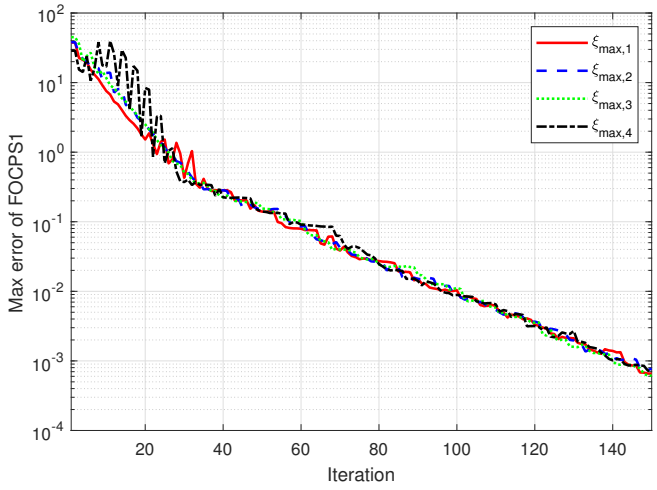


Figure 23. The evolution of maximum distributed output synchronization error $\xi(t)$ for FOCPS1.

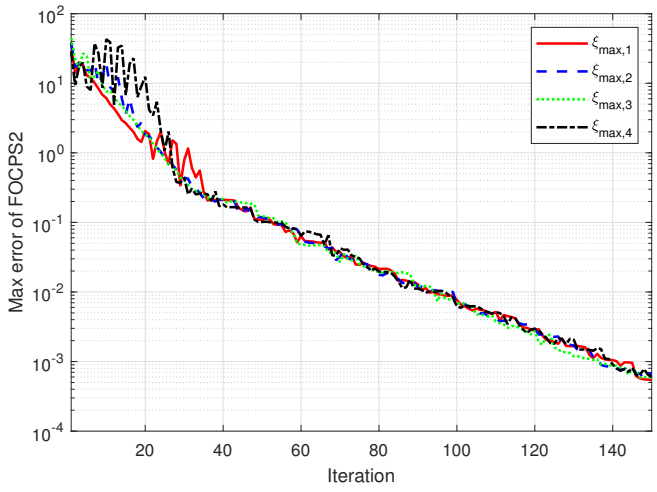


Figure 24. The evolution of maximum distributed output synchronization error $\xi(t)$ for FOCPS2.

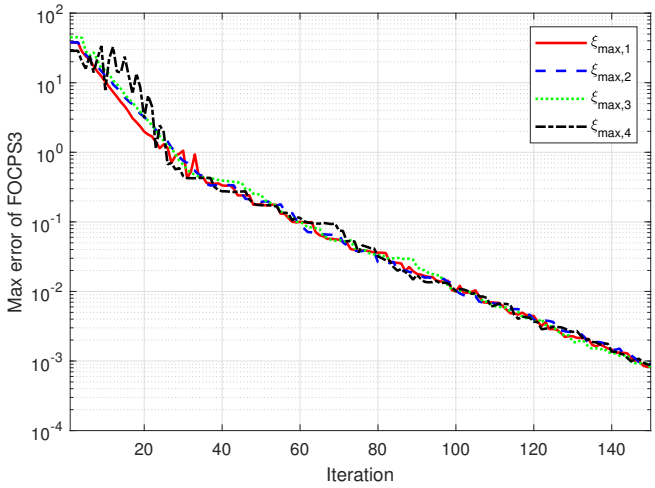


Figure 25. The evolution of maximum distributed output synchronization error $\tilde{\xi}(t)$ for FOCPS3.

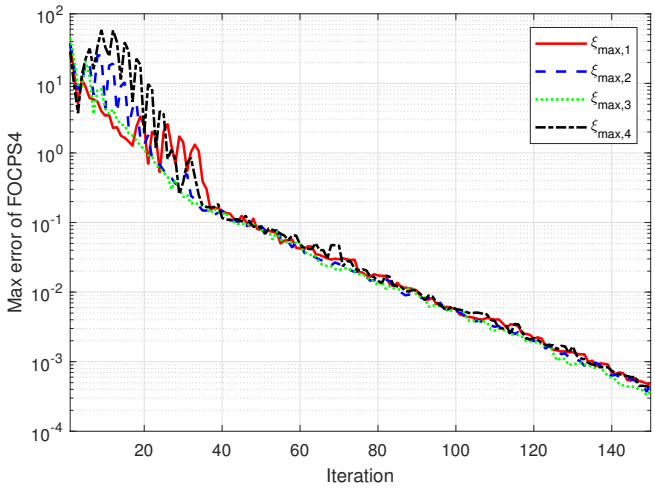


Figure 26. The evolution of maximum distributed output synchronization error $\tilde{\xi}(t)$ for FOCPS4.

Under signal quantization and finite bit-rate communication, the synchronization errors decrease to the order of 10^{-3}, which reflects a relatively small residual error in the tested setting. The similar convergence trends observed in the subplots also indicate that all FOCPSs exhibit comparable synchronization behavior. These numerical results provide support for the applicability of the proposed ET-EDSDILC protocol under the considered communication constraints.

To examine the role of the proposed EDM, a comparative simulation is conducted for the four states of FOCPS1 at the 50th iteration, as shown in Figures 27–30. In the enlarged views, the output without EDM presents a staircase-like profile, which is mainly associated with uncompensated quantization effects under uniform quantization. After incorporating EDM into the control law, the tracking curves become smoother and closer to the desired trajectories. The comparison indicates that the EDM can help reduce the adverse influence of communication quantization in the tested case.

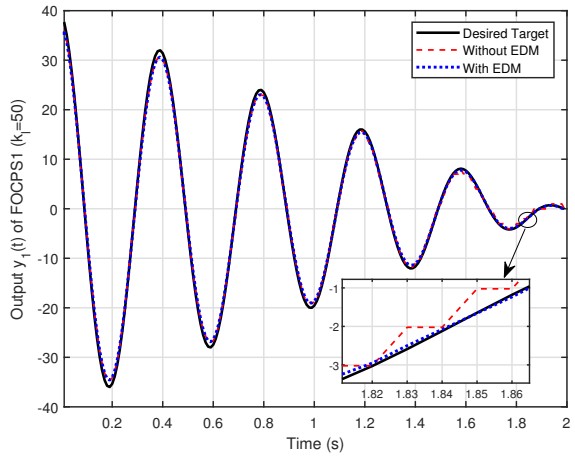


Figure 27. Output synchronization comparison of $y_1(t)$ for FOCPS1 with and without EDM when $k_I = 50$.

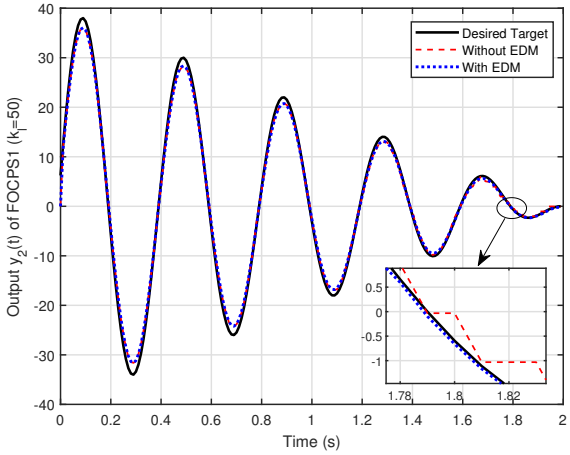


Figure 28. Output synchronization comparison of $y_2(t)$ for FOCPS1 with and without EDM when $k_I = 50$.

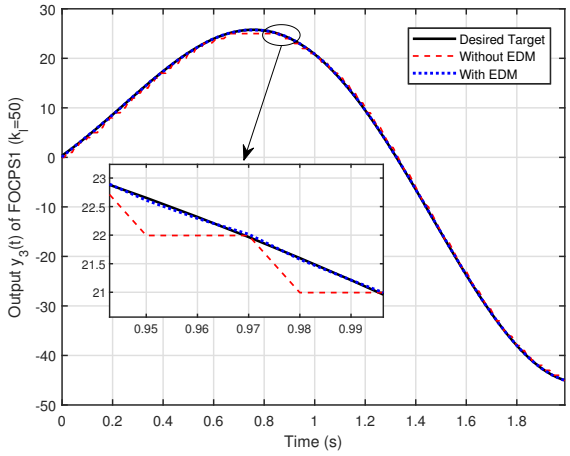


Figure 29. Output synchronization comparison of $y_3(t)$ for FOCPS1 with and without EDM when $k_I = 50$.

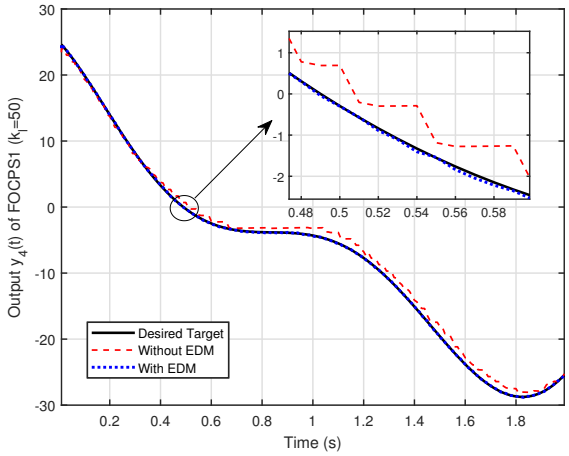


Figure 30. Output synchronization comparison of $y_4(t)$ for FOCPS1 with and without EDM when $k_l = 50$.

To quantitatively examine the overall system behavior, Figure 31 presents the absolute tracking errors of the four states of FOCPS1. Without the EDM, the error curves retain a visible residual bound over the operation interval, which is related to uncompensated quantization noise. When the EDM is included, the errors of the four states are reduced to a narrower neighborhood around zero. This comparison indicates that the EDM contributes to improved steady-state tracking accuracy and more consistent error behavior among the system states in the tested case.

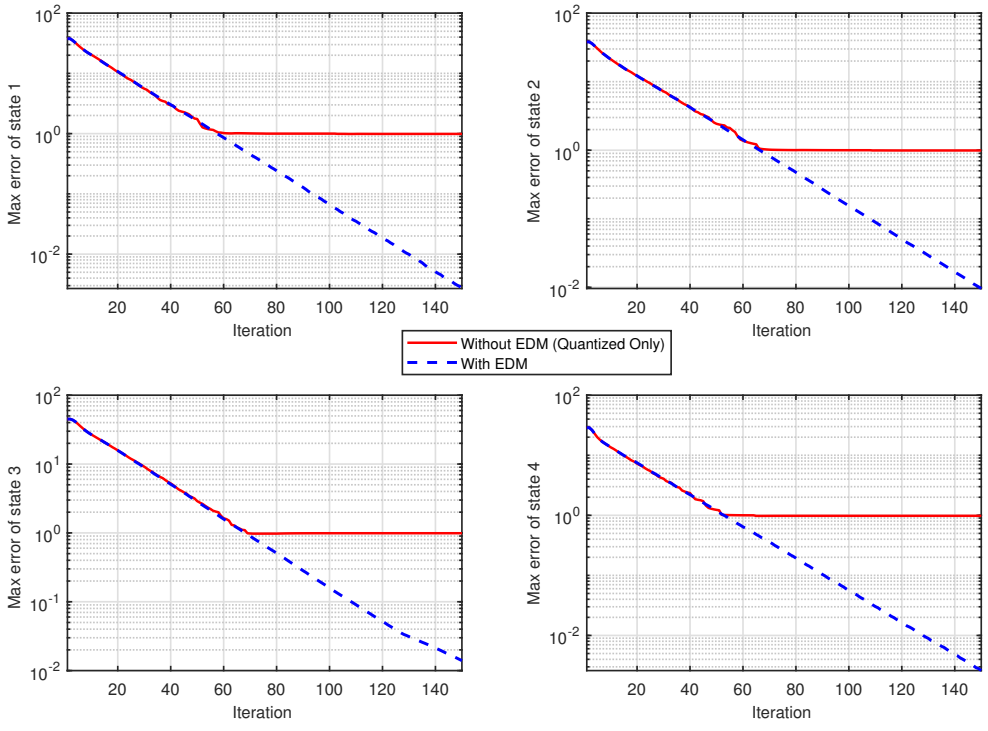


Figure 31. Maximum distributed output synchronization error $\xi(t)$ comparison of FOCPS1 with and without EDM.

7. Conclusions

This research explores the output synchronization problem for FOCPSs under communication constraints. The ET-EDSDILC protocol combines a quantized sampling framework with an encoding–decoding mechanism and an EEA-based event-triggered scheme to

reduce redundant transmissions while aiming to maintain output synchronization despite communication limitations. Theoretical analysis using contraction mapping and fractional-order calculus supports the stability and feasibility of the approach. Numerical simulations suggest that the protocol can reduce communication overhead and data redundancy, providing a reference solution for FOCPSs under communication constraints.

Author Contributions: Conceptualization, J.S. and X.Z. (Xingyu Zhou); methodology, J.S. and S.W.; software, J.S. and X.Z. (Xingyu Zhou); validation, X.Z. (Xinsong Zhang), C.G. and X.Z. (Xingyu Zhou); formal analysis, J.S. and S.W.; investigation, J.S.; resources, X.Z. (Xingyu Zhou) and X.Z. (Xinsong Zhang); data curation, S.W.; writing—original draft preparation, J.S.; writing—review and editing, X.Z. (Xingyu Zhou) and X.Z. (Xinsong Zhang); visualization, J.S. and S.W.; supervision, C.G., X.Z. (Xingyu Zhou) and X.Z. (Xinsong Zhang); project administration, C.G., X.Z. (Xingyu Zhou) and X.Z. (Xinsong Zhang); funding acquisition, C.G., X.Z. (Xingyu Zhou) and X.Z. (Xinsong Zhang). All authors have read and agreed to the published version of the manuscript.

Funding: This work was partially supported by the Natural Science Foundation of Jiangsu Province (No. BK20250961), the Natural Science Research of Jiangsu Higher Education Institutions of China (No. 24KJB120012), and the National College Students' Innovation and Entrepreneurship Training Project (Nos. 202510304088 and S202510304156).

Data Availability Statement: All necessary data utilized in this article are comprehensively incorporated within its contents.

Conflicts of Interest: The authors declare that they have no conflicts of interest.

References

1. Hasan, M.K.; Hasan, M.M.; Awouda, A.E.; Mokhtar, U.A.; Islam, S.; Elshafie, H.; Saeed, R.A.; Ghazal, T.M. Smart grid cyber-physical systems: Components, vulnerabilities, mitigations, opportunities, and conceptual framework. *Energy Rep.* **2026**, *15*, 109255. [CrossRef]
2. Yu, R.; Liu, M.; Zhu, W.; Chen, Y.H.; Zhang, X. Robust control design for nonlinear cyber-physical systems: Application to the U-turn in autonomous vehicles. *Nonlinear Dyn.* **2025**, *113*, 6997–7011.
3. Chen, C.; Yan, J.; Lu, N.; Wang, Y.; Yang, X.; Guan, X. Ubiquitous monitoring for industrial cyber-physical systems over relay-assisted wireless sensor networks. *IEEE Trans. Emerg. Top. Comput.* **2015**, *3*, 352–362.
4. Luo, X.; Zhang, D.; Yang, L.T.; Liu, J.; Chang, X.; Ning, H. A kernel machine-based secure data sensing and fusion scheme in wireless sensor networks for the cyber-physical systems. *Future Gener. Comput. Syst.* **2016**, *61*, 85–96. [CrossRef]
5. Xiong, M.; Tan, Y.; Du, D.; Zhang, B.; Fei, S. Observer-based event-triggered output feedback control for fractional-order cyber-physical systems subject to stochastic network attacks. *ISA Trans.* **2020**, *104*, 15–25. [CrossRef] [PubMed]
6. Sharafian, A.; Ullah, I.; Singh, S.K.; Ali, A.; Khan, H.; Bai, X. Adaptive fuzzy backstepping secure control for incommensurate fractional order cyber–physical power systems under intermittent denial of service attacks. *Chaos Solitons Fractals* **2024**, *186*, 115288. [CrossRef]
7. Ma, J.; Xu, X.; Wang, G.; Cai, S.; Zhou, X.; Zhang, S. Iterative Learning Fault Diagnosis of Fractional-Order Nonlinear Multi-Agent Systems with Initial State Learning and Switching Topology. *Fractal Fract.* **2026**, *10*, 106.
8. Zhang, X.; Li, X.; Yang, K.; Wang, Z. Lithium-ion battery modeling and state of charge prediction based on fractional-order calculus. *Mathematics* **2023**, *11*, 3401.
9. Chen, W.; Zhou, B.; Wang, H. On Controllability of Transportation Networks with Fractional-Order Dynamics. In *Proceedings of the 2021 International Conference on Neuromorphic Computing (ICNC)*; IEEE: Piscataway, NJ, USA, 2021; pp. 338–344.
10. Xu, J.X.; Yan, R. Iterative learning control design without a priori knowledge of the control direction. *Automatica* **2004**, *40*, 1803–1809. [CrossRef]
11. Moore, K.L.; Chen, Y.; Bahl, V. Monotonically convergent iterative learning control for linear discrete-time systems. *Automatica* **2005**, *41*, 1529–1537. [CrossRef]
12. Meng, D.; Moore, K.L. Convergence of iterative learning control for SISO nonrepetitive systems subject to iteration-dependent uncertainties. *Automatica* **2017**, *79*, 167–177. [CrossRef]
13. Li, Y.; Chen, Y.; Ahn, H.S. Fractional-order iterative learning control for fractional-order linear systems. *Asian J. Control* **2011**, *13*, 54–63. [CrossRef]
14. Wang, Y.; Zhou, F.; Yin, L.; Wan, F. Iterative learning control for fractional order linear systems with time delay based on frequency analysis. *Int. J. Control Autom. Syst.* **2021**, *19*, 1588–1596. [CrossRef]

15. Shi, T.; Che, W.W. Robust data-driven iterative learning control for nonlinear cyber-physical systems. *Int. J. Robust Nonlinear Control* **2023**, *33*, 8433–8451. [CrossRef]
16. Wang, Z.; Tang, S.; Guo, G.; Yang, Y.; Han, M.; Yang, L.; He, D. Event-triggered data- and knowledge-driven adaptive quality iterative learning control with uncertainty for a pharmaceutical cyber-physical system. *Can. J. Chem. Eng.* **2023**, *101*, 5844–5857. [CrossRef]
17. Song, X.; Liu, S.; Wang, M.; Zhu, C.; Song, D.; Song, S. Sampled-data event-triggered resilient consensus control of multiple flexible manipulators with actuator failures via iterative learning scheme. *ISA Trans.* **2026**, *169*, 128–136. [CrossRef] [PubMed]
18. Xiong, W.; Yu, X.; Patel, R.; Yu, W. Iterative learning control for discrete-time systems with event-triggered transmission strategy and quantization. *Automatica* **2016**, *72*, 84–91. [CrossRef]
19. Wang, X.; Qin, W.; Park, J.H.; Shen, M. Event-triggered data-driven control of discrete-time nonlinear systems with unknown disturbance. *ISA Trans.* **2022**, *128*, 256–264. [CrossRef] [PubMed]
20. Strijbosch, N.; Oomen, T. Iterative learning control for intermittently sampled data: Monotonic convergence, design, and applications. *Automatica* **2022**, *139*, 110171. [CrossRef]
21. Chen, F.M.; Tsai, J.S.H.; Liao, Y.T.; Guo, S.M.; Ho, M.C.; Shaw, F.Z.; Shieh, L.S. An improvement on the transient response of tracking for the sampled-data system based on an improved PD-type iterative learning control. *J. Frankl. Inst.* **2014**, *351*, 1130–1150. [CrossRef]
22. Zhao, X.; Wang, Y. Distributed point-to-point iterative learning control for multi-agent systems with quantization. *J. Frankl. Inst.* **2021**, *358*, 6508–6525. [CrossRef]
23. Tao, Y.; Tao, H.; Zhuang, Z.; Stojanovic, V.; Paszke, W. Quantized iterative learning control of communication-constrained systems with encoding and decoding mechanism. *Trans. Inst. Meas. Control* **2024**, *46*, 1943–1954. [CrossRef]
24. Zhang, C.; Shen, D. Zero-error convergence of iterative learning control based on uniform quantisation with encoding and decoding mechanism. *IET Control Theory Appl.* **2018**, *12*, 1907–1915. [CrossRef]
25. Zhang, K.; Zhang, H.; Liang, X.; Wang, Z. Neurodynamic programming and tracking control scheme of constrained-input systems via a novel event-triggered PI algorithm. *Appl. Soft Comput.* **2019**, *83*, 105629. [CrossRef]
26. Piqueira, J.R.C.; Alsinai, A.; Niazi, A.U.K.; Jamil, A. Distributed delay control strategy for leader-following cyber secure consensus in Riemann–Liouville fractional-order delayed multi-agent systems under denial-of-service attacks. *Partial Differ. Equ. Appl. Math.* **2024**, *11*, 100871.
27. Daftardar-Gejji, V.; Jafari, H. Analysis of a system of nonautonomous fractional differential equations involving Caputo derivatives. *J. Math. Anal. Appl.* **2007**, *328*, 1026–1033. [CrossRef]
28. Yu, R.; Zhang, H. New function of Mittag-Leffler type and its application in the fractional diffusion-wave equation. *Chaos Solitions Fractals* **2006**, *30*, 946–955.
29. Kim, Y.H. Gronwall, Bellman and Pachpatte type integral inequalities with applications. *Nonlinear Anal. Theory Methods Appl.* **2009**, *71*, e2641–e2656. [CrossRef]

Disclaimer/Publisher's Note: The statements, opinions and data contained in all publications are solely those of the individual author(s) and contributor(s) and not of MDPI and/or the editor(s). MDPI and/or the editor(s) disclaim responsibility for any injury to people or property resulting from any ideas, methods, instructions or products referred to in the content.